Structural Comparison Study of (6-4) Photolyase from *Vibrio cholerae*

by

Barış Çakılkaya

A Dissertation Submitted to the
Graduate School of Sciences and Engineering
in Partial Fulfillment of the Requirements for
the Degree of

Master of Science

in

Molecular Biology and Genetics

KOÇ
ÜNİVERSİTESİ

July 26, 2022

Structural Comparison Study of (6-4) Photolyase from *Vibrio cholerae*

Koç University

Graduate School of Sciences and Engineering

This is to certify that I have examined this copy of a master's thesis by

Barış Çakılkaya

and have found that it is complete and satisfactory in all respects,
and that any and all revisions required by the final
examining committee have been made.

Committee Members:

Prof. İ. Halil Kavaklı (Advisor)

Assist. Prof. Hasan Demirci (Co-Advisor)

Assist. Prof. Serkan Kır

Prof. Nuri Öztürk

Assist. Prof. Cihan Aydın

Date: 26.07.22

To my beloved heroes…

ABSTRACT

Upon Ultraviolet (UV) irradiation to the DNA, pyrimidine dimers are formed. These mutagenic lesions are either in form of cyclobutene pyrimidine dimers (CPD) or (6-4) photoproducts ((6-4) PPs). Photolyases (PLs) are DNA repair enzymes that use blue light energy to catalyze pyrimidine dimers back to their original state. PLs are named after their specific substrates and their repair functions. (6-4) PLs repair (6-4) PPs with the help of catalytic cofactor flavin adenine dinucleotide (FAD) and an additional antenna chromophore. Bacterial (6-4) PLs contain another cofactor called [4Fe-4S] cluster with an unknown function.

In this study, the crystal structure of (6-4) photolyase from *Vibrio cholerae* (O1 bivar Tor str. N16961) *(Vc)* has been identified at 2.5 Å resolution. The presence and location of FAD, 6,7-dimethyl-8-ribityllumazine (DMRL), and [4Fe-4S] cofactors were shown by the electron clouds. Their interactions with the *Vc*(6-4) PL were investigated with the comparison of other structurally available bacterial (6-4) PLs and *Drosophila melanogaster (Dm)* (6-4) PL. The comparison revealed a conserved water molecule that might be stabilizing the DMRL in bacterial PLs, which makes tighter interaction in *Vc*(6-4) PL. In a conserved motif located at the catalytic domain, a different conformation was observed between *Vc*(6-4) PL and *Dm*(6-4) PL residue. A disordered region in the *Vc*(6-4) PL was observed and suggested as a DNA binding site. A structural comparison with *Dm*(6-4) PL revealed that *Vc*(6-4) PL has two additional helixes in C-terminal. Further computational studies suggest either DNA binds to *Vc*(6-4) PL in a different manner than *Dm*(6-4) PL or *Vc*(6-4) PL might be subjected to a conformational change upon DNA binding.

ÖZETÇE

DNA'ya Ultraviyole (UV) ışınlaması üzerine, pirimidin dimerleri oluşur. Bu mutajenik lezyonlar ya siklobuten pirimidin dimerleri (CPD) ya da (6-4) fotoürünleri ((6-4) PP'ler) şeklindedir. Fotoliyazlar (PL'ler), pirimidin dimerlerini orijinal durumlarına geri katalize etmek için mavi ışık enerjisini kullanan DNA onarım enzimleridir. PL'ler, belirli alt katmanlarından ve onarım işlevlerinden sonra adlandırılır. (6-4) PL'ler, katalitik kofaktör flavin adenin dinükleotidi (FAD) ve ek bir anten kromoforu yardımıyla (6-4) PP'leri onarır. Bakteriyel (6-4) PL'ler, bilinmeyen bir işleve sahip [4Fe-4S] kümesi adı verilen başka bir kofaktör içerir.

Bu çalışmada, *Vibrio cholerae* (O1 bivar Tor str. N16961) (*Vc*) kaynaklı (6-4) fotolizazın kristal yapısı 2.5 Å çözünürlükte tanımlanmıştır. FAD, 6,7-dimetil-8-ribitylumazin (DMRL) ve [4Fe-4S] kofaktörlerinin varlığı ve konumu elektron bulutları tarafından gösterildi. Bu kofaktörlerin *Vc*(6-4) PL ile etkileşimleri, yapısal olarak mevcut diğer bakteriyel (6-4) PL'ler ve *Drosophila melanogaster* (*Dm*) (6-4) PL'in karşılaştırılmasıyla araştırıldı. Karşılaştırma, bakteriyel PL'lerde DMRL'ı stabilize edebilen ve *Vc*(6-4) PL'de daha sıkı etkileşim sağlayan korunmuş bir su molekülünü ortaya çıkardı. Katalitik alanda bulunan korunmuş bir motifte, *Vc*(6-4) PL ve *Dm*(6-4) PL tortusu arasında farklı bir konformasyon gözlemlendi. *Vc*(6-4) PL'de düzensiz bir bölge gözlemlendi ve burası bir DNA bağlanma bölgesi olarak önerildi. *Dm*(6-4) PL ile yapısal bir karşılaştırma, *Vc*(6-4) PL'nin C-terminalinde iki ek sarmal olduğunu ortaya çıkardı. Ek hesaplama çalışmaları, DNA'nın *Vc*(6-4) PL'ye *Dm*(6-4) PL'den farklı bir şekilde bağlandığını veya *Vc*(6-4) PL'nin DNA bağlanması üzerine bir konformasyonel değişikliğe maruz kalabileceğini ileri sürmektedir.

ACKNOWLEDGEMENTS

I would like to thank Prof. Halil Kavaklı for accepting me as an undergrad in his lab and allowing me to start my academic carrier. I would like to thank Dr. Hasan Demirci for giving me the opportunity to do amazing science in his lab and for all the delicious sushi that I ate without a second thought. I appreciate Prof. Nuri Öztürk, Dr. Cihan Aydın, and Dr. Serkan Kır for spending their time on my thesis and giving feedback. I would like to thank Koç University for being a home for me for 8 years and TÜBITAK 2232 International Fellowship for Outstanding Researchers Program (Project No: 118C270) for the financial support.

First, I would like to mention Melis Çelik for her constant support for 8 years. Through your companionship, I was able to come this far and have the bravery to continue even further. You were there to show me light in my darkest times, and I feel so lucky to have you in my life. If I ever fell, I know that Melis will be right behind me to back me up on my feet again. You are a very brilliant person, and I aim to be like you. I am so glad that you are in my life, and I hope this won't ever change.

I would like to mention my bud Samet Ağca for all the fun and academic help over the years. I don't think I could have gotten my diploma without your help in literally every single course I have taken. For 8 years, Koç University was my home, and you were the constant in this home. Thank you for everything you have done for me.

I would like to thank the amazing person Zeynep Melis Gül for all the help that she provided. You are such an easy-going person, and I am so happy to know you. I really appreciate your willingness to support your surroundings, and thanks to you, I never felt alone in the lab.

I would like to thank Gizem Çağla Parlak for being the fun of the lab. You were an oasis in the middle of all the stress and suffering of academic life. I am so grateful for all the laughs and enjoyment we shared together. I hope all the best for your life.

I really appreciate one of the kindest person, Mehmet Gül for his friendship. Our hangouts were much needed cool offs and I thank you for every second of it. It was very nice to have a second home with the most welcoming host and away from all the negativities. I am really grateful for everything and will be waiting for you on your next step.

I would like to thank Onur Özcan for all the help and scientific discussions while being extremely patient, Bilge Bahar Çamur for being an excellent mentor, and all the Kavaklı lab members for their honesty and professionality.

I would like to thank the Büşra Yüksel for all the fun times we have shared. It is truly a unique experience to hang out with you, and I hope we can carry this energy to next step of our academic carrier.

I would like to thank outstanding Betül Ertem, the brightest Alaleh Shafiei, Nurettin Tokay, Destan, and all the Demirci Lab members for being amazing characters. I have learned a lot in the laboratory, and I will definitely remember every aspect of it.

And last but not least, I would like to thank my besty group members, the chairwoman Minel Güler, the messenger Melike Çoşkun, the expert Hilal Öztürk, and the doctor Büşra İzgi Ağca. I cannot imagine my university life without you, and I felt Koç University was my home because you guys were here with me. I really appreciate all the adventures we have experienced together and all the beautiful memories we have collected. I feel privileged to be in this group, and no matter how much distance will separate us, we will be together. I love all of you.

TABLE OF CONTENTS

LIST OF TABLES

LIST OF FIGURES

ABBREVIATIONS

(6-4) PP	Pyrimidine-pyrimidone (6-4) photoproducts
[4Fe-4S]	4 iron-4 sulfur cluster
8-HDF	8-hydroxy-5-deazariboflavin
Å	Armstrong
CFE	Cell free extract
CPD	Cyclobutane pyrimidine dimers
CRY	Cryptochrome
Da	Dalton
DMRL	6,7-dimethyl-8-ribityl lumazine
FAD	Flavin adenine dinucleotide
FMN	Flavin mononucleotide
FRET	Fluorescence resonance energy transfer
h	hour
IPTG	Isopropyl- β-D-1-thiogalactopyranoside
L	Liter
M	Molarity
Min	Minutes
mg	milligram
MTHF	5,10-methenyltetrahydrofolate
nm	Nanometer
PDB	Protein data bank
PL	Photolyase
S	Seconds
Un	Uninduced
UV	Ultraviolet
WCL	Whole cell lysate
α	Alpha
β	Beta

Chapter 1:
INTRODUCTION

Upon UV light irradiation, adjacent pyrimidines form dimers which are highly mutagenic [1]. If not repaired, they may lead to death of the organism, eukaryote or prokaryote alike. Depending on the interaction between the pyrimidines, cyclobutene pyrimidine dimers (CPD) or pyrimidine-pyrimidone (6-4) products. Many organisms deal with UV from the Sun by using DNA repair enzymes that are specifically repairing UV induced DNA lesions. Photolyases are UV induced DNA repair enzymes that uses blue light energy to repair the lesion without requiring any other protein or energy source. Depending on the substrate binding affinity, photolyases are divided into two main groups, CPD PLs and (6-4) PLs [2].

Photolyases are flavoprotein that interacts with blue light to repair DNA lesions. The photolyases contain various types of cofactors depending on the organism and photolyase type. However, FAD is the catalytic cofactor for the repair, and it is present in every single photolyase. There are additional antenna chromophores that has higher excitation coefficient under the blue light. These chromophores can be MTHF, DMRL, or 8-HDF and they can transfer its energy to the FAD by FRET mechanism. Upon excitation, FAD is reduced to $FADH^{-\cdot}$ and initiates the electron transfer to the lesion, which breaks bond between the carbons [3].

Studies have shown that *Vibrio cholerae* (O1 bivar Tor str. N16961) has a very particular blue light response, which heavily regulates the transcription of many genes. Total of 4 genes have been identified as a photolyase which contains 1 CPD, 2 single stranded photolyase and 1 (6-4) photolyase [4] . Interestingly, (6-4) photolyase contains an additional cofactor called [4Fe-4S] cluster that is unique to bacterial (6-4) PL family [5]. Current studies failed to show its function; however, mutagenesis assays suggest its stability function[6].

In this study, we have crystalized the (6-4) photolyase from *Vibrio cholerae* and solved its structure at 2.5 Å resolution. The structure revealed the presence and binding interaction of DMRL, FAD, and [4Fe-4S] cluster with the photolyase. We have identified a conserved water molecule around the DMRL, which might regulate the binding of the DMRL bacterial (6-4) PLs. Structural comparison studies revealed that, conserved motif around the FAD has slight differences, and such conformation change might indicate a

different function. Our [4Fe-4S] cluster was undamaged even after months of atmospheric condition which may suggest its high tolerance to the oxygenic environment. According to our structural and computational studies, we suggest a DNA binding region between 478-485 amino acid residues. Our further studies revealed that DNA lesion might be binding to the *Vc*(6-4) PL differently than *Dm*(6-4) PL or there might a conformational change at PL on DNA binding.

Chapter 2 is the review of UV-induced DNA damages and their repairment by the photolyases.

Chapter 3 shows materials and methods that is used in this study.

Chapter 4 shows the results of the study.

Chapter 5 include discussion of the results and findings on the study.

Chapter 2:
LITERATURE REVIEW

2.1 UV light induced DNA damage

Ultraviolet (UV) light is defined as 100 to 400nm wavelength in the electromagnetic spectrum. In nature, main source of UV on earth is the Sun and the surface of the earth is protected by the oxygen and the ozone layer in the atmosphere. UVC (100-280nm) is the most energetic and dangerous UV light, and it is highly absorbed by the molecular oxygen (O_2) and the ozone (O_3) layer therefore, it is irrelevant for the ecosystems. UVB (280-315nm) is mostly absorbed by the ozone layer however, some of them reach to the surface of the earth and interacts with living matters. UVA (315-400nm) has the lowest energy and not absorbed by the atmosphere however, it is less efficient to induce damage on cells [1].

The UV light causes damage on DNA where two adjacent pyrimidines make covalent bonds with each other. Depending on the interaction between the pyrimidines, the lesion is called cyclobutane pyrimidine dimers (CPDs) or 6-4 photoproducts (6-4 PPs) (Figure 2.1). CPDs are the most abundant upon UV exposure, however both types are mutagenic and potentially lethal. In CPDs, four-member ring is formed between C5 and C6 of the two adjacent pyrimidines. In case of 6-4 PPs, a bond is formed between C6 from 5' end pyrimidine to C4 of the other pyrimidine. While the bonding occurs, oxetane from 3'end of thymine or azetidine from 3'end of cytosine rearranges into pyrimidine at 5'end [7].

Dewar isomers are formed with 6-4 PPs when the lesion exposed to UVA which can be transferred back to 6-4 PP by the UVC irradiation [8].

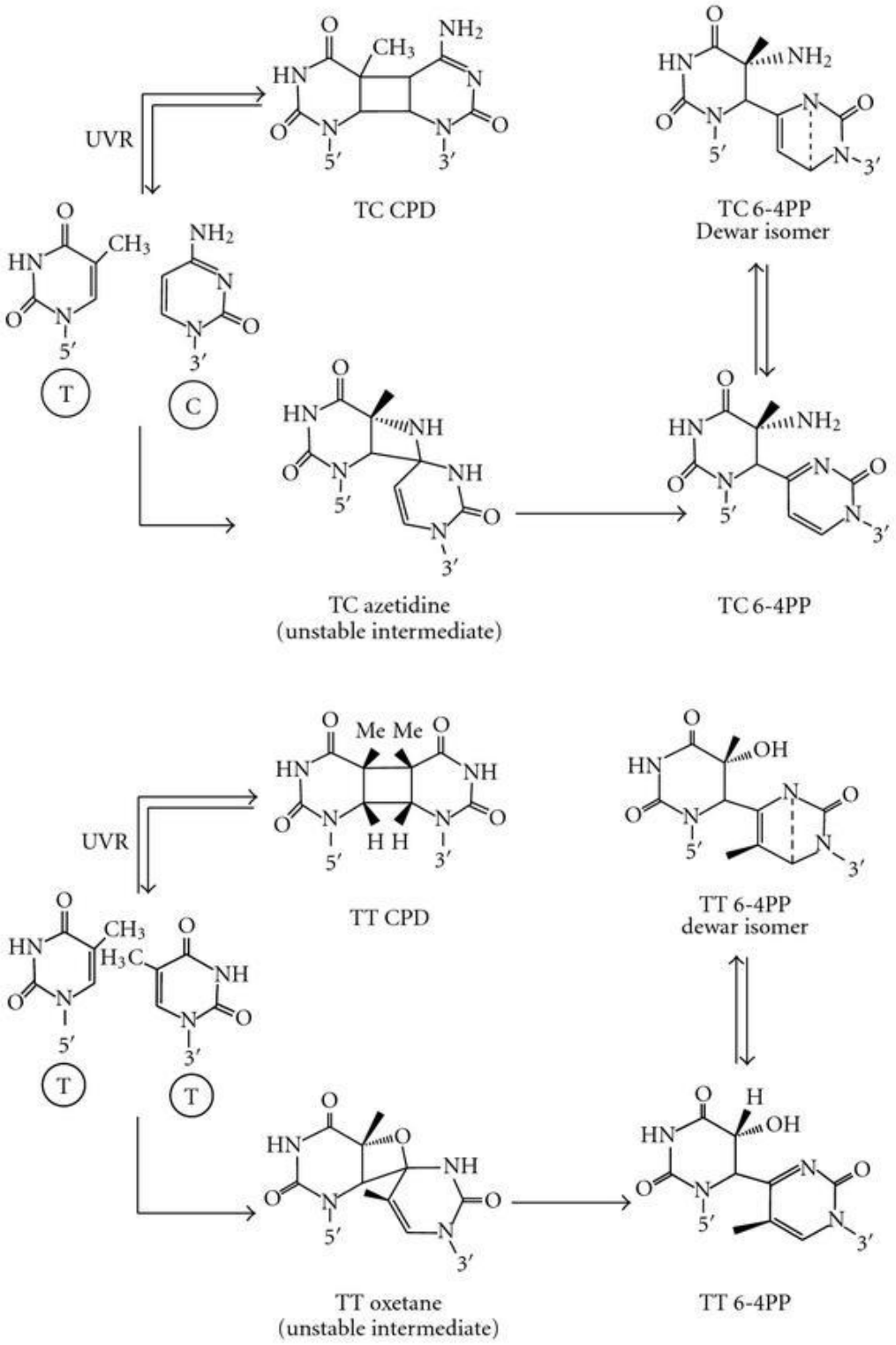

Figure 2.1: UV-induced DNA damages to two adjacent pyrimidines. Top part represents the thymine-cytosine photoproducts. Bottom part is for Thymine-thymine CPD and (6-4) PP formation. Reprinted with the permission from [9].

Upon UV-induced DNA damage, around 75% of the damaged products are CPDs while around 25% of the damaged products are 6-4 PPs. Regardless of the type of the lesion, DNA helix is distorted, and bend or kink is formed. DNA polymerase activity is inhibited by the formation of CPD lesions [1].

2.2 Photolyases

2.2.1 Blue light receptors

Most living organisms is capable of sensing and responding to blue light (400-500 nm). The earliest studies of light sensitivity were on plants which gave different reactions depending on the color of the light [10]. The growth speed of the plant was changing by the light color and nourishment was the highest with the lower wavelength colors. Later, specific blue light responses were identified in the plants as well as other types of organisms [11], [12].

Light quantity and the light properties change according to the habitat of the organism. Especially aquatic organisms mainly subjected to blue light and UV radiation due to them being only type of light source that can penetrate to the depths [13]. Marine organisms have sophisticated blue light receptors to adapt the environment and response accordingly.

2.2.2 Photolyases

UV light was used as a sterilization tool even before its effect on the DNA. However, it is observed by Albert Kerber in 1949 that upon visible light radiation after the UV, the bacteria culture come back alive [14]. This phenomenon is called photoreactivation, and later Dr. Rubert is defined the DNA damage of the UV light and hypothesized a protein called photolyase that repairs these damages by using the blue light [15]. Depending on the substrate of the enzyme, they are named either CPD, CRY-DASH, or (6-4) photolyases. One of the cofactors in the protein is flavin adenine dinucleotide (FAD) [16]. The enzyme has different colors depending on the redox state of FAD, which can change colors to purple to orange [17].

2.2.3 Structure of photolyases

Photolyases are monomeric proteins that are found in various organisms including fungi, bacteria, plants and a large range of animals. The size of the photolyases is in between 50 kDa and 61 kDa, with the amino acid ranging between 420-616 [18], [19]. Photolyases contain two domains which are called α-helical domain and α/β domain and the two domains are connected by the loop region. α-helical domain contains FAD while the α/β domain contains the secondary chromophore, which changes depending on the photolyase [8]. From the non-covalently bound cofactors, FAD is the essential one for the repair activity. The antenna chromophore, which can be 6,7-dimethtyl 8-ribityl-lumazin (DMRL), methenyltetrahydrofolate (MTHF), 8-hydroxy-7,8-didemethyl-5-deazariboflavin (8-HDF), and flavin mononucleotide (FMN) are non-essential which is shown by the mutagenesis studies [20].

2.2.4 CPD photolyases

The first photolyase structure was from E. coli CPD photolyase that is deposited to the Protein Data Bank (PDB) [21]. The structure is solved at 2.3 Å (PDB ID: 1DNP) and its ribbon representation and calculated surface charge can be seen in **Figure 2.2**. The structure revealed the domains and the cofactor interactions of the photolyase. MTHF was the antenna chromophore in the α/β domain and FAD has a unique U-shaped conformation in the α-helical domain. MTHF get excited by the blur light can transfer the energy to the FAD by using Förster resonance energy transfer (FRET). Similar with other photolyases, the distance between two factors is around 16 Å, which allows energy transfer from antenna cofactor to catalytic cofactor FAD.

Positively charged residues around the FAD and the α-helical domain to thought to be interacting with the DNA. Later years, DNA binding interactions were shown by the crystal structure of the CPD photolyase from *Anacystis nidulans* that contains CPD photoproduct (PDB ID: 1TEZ) [22]. The structure revealed that the lesion part is flipped out towards the catalytic cofactor FAD by the interaction of amino acids.

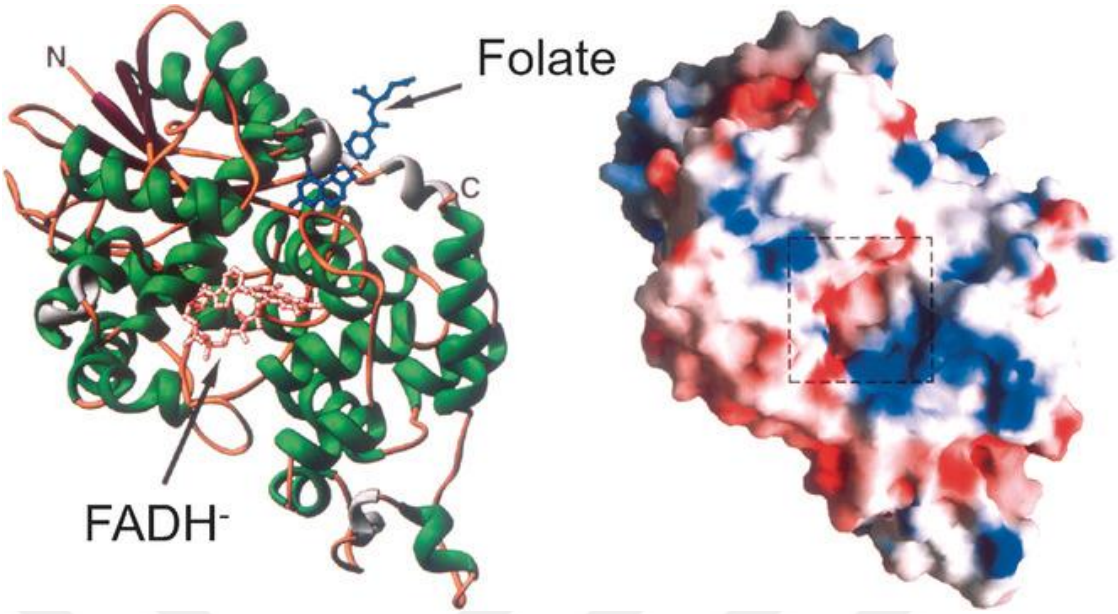

Figure 2.2: Crystal structure of *E. coli* CPD photolyase. Left figure is ribbon representation of photolyase with cofactors. Right is the surface charge of protein. Reprinted from the reference [23] with permission.

2.2.5 CRY-DASH photolyases

CRY-DASH proteins are specialized in repairing single stranded CPD lesion in DNA. Similar to other photolyases, they present in many other organisms with variety of additional functions [24]. They are called cryptochromes due to failed attempts to show their repair activity with double stranded DNA lesions [25]. Later studies showed its photolyase activity to ss DNA lesion with high specificity toward CPDs [26]. Interestingly, studies revealed multiple CRY-DASH proteins present in some organisms, which indicates their further importance to the cells [27], [28].

2.2.6 (6-4) photolyases

The first identification of (6-4) photolyase has been done on *Drosophila melanogaster* in 1993 by Todo et al. [29]. Although its repair function has been shown, substrate binding mechanism were missing. In 2008, Maul et al. cocrystallized the *Dm(*6-4) PL with T-T (6-4) PP (PDB ID: 3CVU) and repaired version (PDB ID: 3CVY) [30].

The structure revealed the important interaction partners of the DNA lesion and give some light to repair mechanism of the enzyme (**Figure 2.3**).

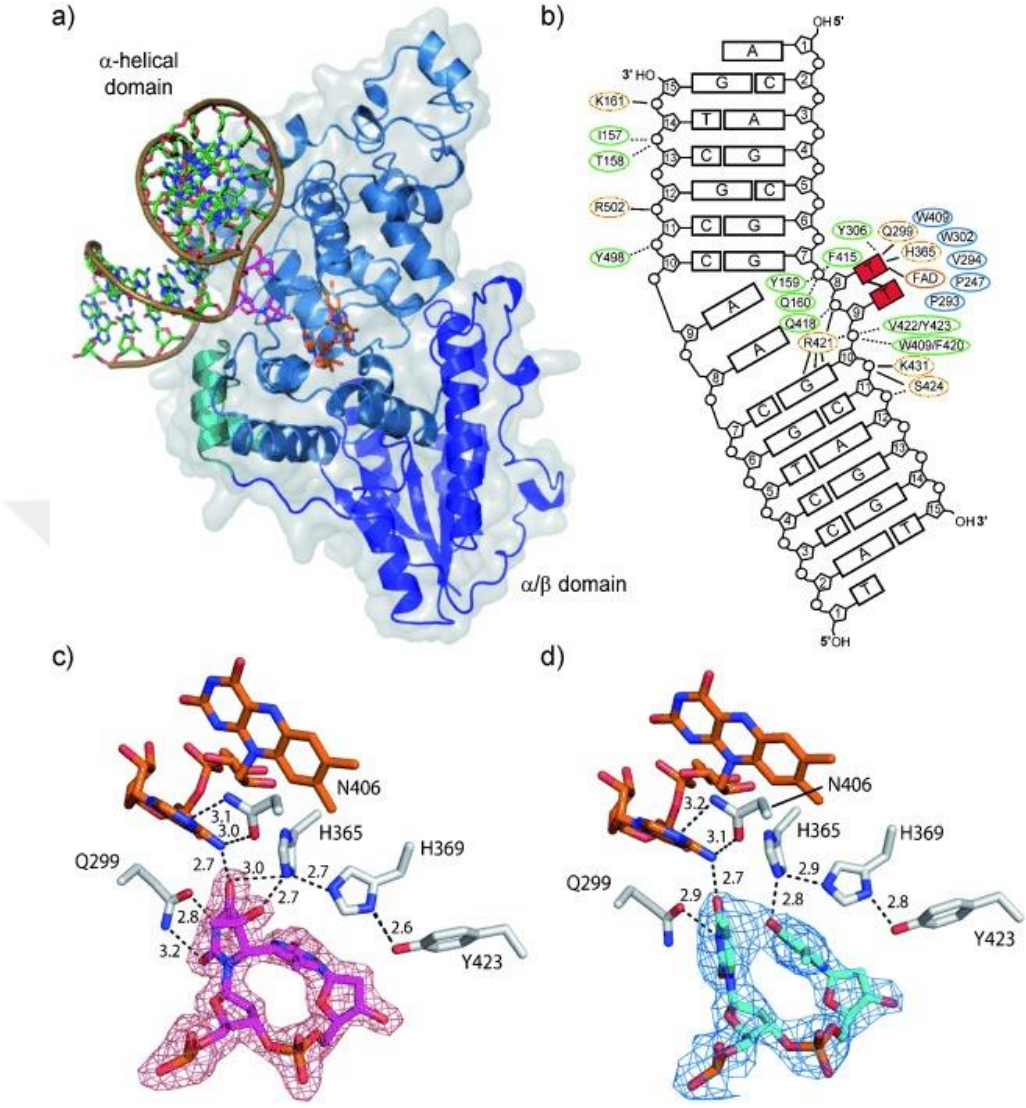

Figure 2.3: Crystal structure and DNA lesion interactions of *Dm*(6-4) PL. a) Structure overview of *Dm*(6-4) PL. b) DNA lesion interactions of PL. c) DNA lesion interactions of catalytic domain. d) Repaired DNA interactions of catalytic domain. Reprinted from the reference [30] with permission.

For a long time, (6-4) photolyases thought to be present only in eukaryotes. This was changed when (6-4) PP repair activity has been shown by a (6-4) photolyase from *Agrobacterium tumefaciens* [31]. In the study, they solved the structure at 1.45 Å resolution and identified 3 cofactors. Similar to other photolyases, catalytic cofactor FAD and antenna chromophore DMRL was present with an additional [4Fe-4S] cluster cofactor. Overview of the structure showed the two main domains, α/β domain and α-helical domain, are present similar to other photolyases. On the phylogenetic tree,

bacterial [4Fe-4S] cluster has the highest distance to any other type of photolyase [27]. Due to their sequence difference, identification of bacterial (6-4) photolyase took years to accomplished.

The [4Fe-4S] cluster in the bacterial (6-4) PL are located in between 4 Cytosine residues which are interacting with the Fe atoms of the cluster. The cluster is also located in the α-helical domain, with the unknown function of protein stability or the electron transfer. Mutagenesis analysis on the *At*(6-4) PL has shown that, without the Cys residues that interact with the [4Fe-4S] cluster, the protein expression heavily crippled. Some expressed photolyase observed in the insoluble fraction and function of the [4Fe-4S] cluster in the bacterial photolyases has suggested as the protein stability and proper folding [6].

2.2.7 Iron-sulfur clusters

Studies have shown that, (Fe-S) cluster are essential part of the nucleic acid machinery. They are found as cofactors in some of the primases, helicases, transcription factors, and transferases [32]. Regardless of the protein, they are all interact with cysteine residues. Depending on the enzyme, they may have electron transfer or stabilize DNA interaction with the enzyme by changing redox states [33].

There are 3 main types of iron-sulfur clusters which are defined by their number of iron atoms in the cluster. The structures of [2Fe-2S], [3Fe-4S], and [4Fe-4S] clusters can be seen in **Figure 2.4**. Although they are very useful and essential inorganic compounds for many organisms, they have limiting factors. One of the main issues is the iron must be available in the environment, which for many organisms, it may not be so abundant. Another main issue is the oxidation of irons the in the cluster which converts $[4Fe\text{-}4S]^{+2}$ into $[4Fe\text{-}4S]^{+3}$. The $[4Fe\text{-}4S]^{+3}$ cluster is highly unstable and will quickly lose its iron and lose its catalytic function. Upon longer exposure times with oxygen, the cluster can dissociate into [2Fe-2S] cluster and later completely dissociates [34].

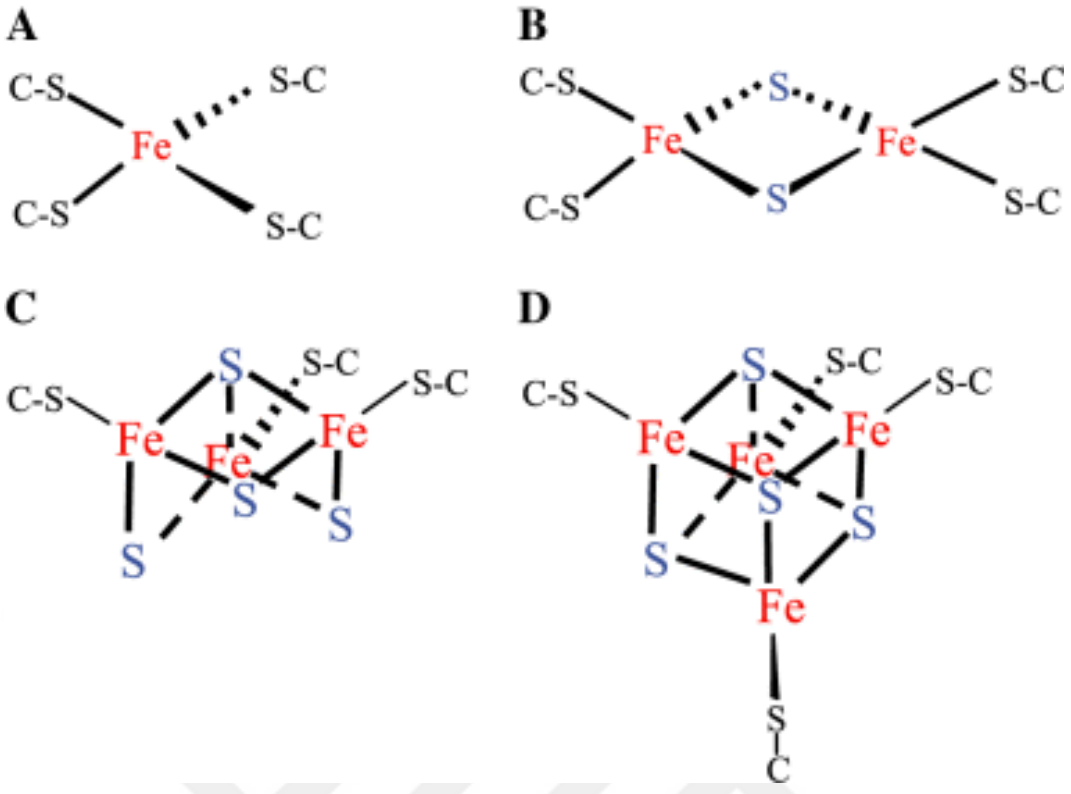

Figure 2.4: Structure of iron-sulfur clusters. A) Structure of iron cluster B) Structure of [2Fe-2S] cluster. C) Structure of [3Fe-4S] cluster. D) Structure of [4Fe-4S] cluster. Reprinted from reference [34] with permission.

2.2.8 Photoreduction of FAD

The catalytic cofactor has total of 3 redox states called fully reduced, semireduced, and oxidized states. Fully reduced state has $FADH^-$ and $FADH_2$ forms, which can oxidize into $FADH^{\cdot}$ and further into $FAD^{\cdot-}$ forms, which are semireduced states. Oxidized state has a single from which is FAD [35]. Each redox state their own UV-vis absorption pattern which can be seen in **Figure 2.5**. Although FAD has a number of different redox states, $FADH^-$ is only active state where the DNA repair can occur [36]. The reduction is done by the help of the blue light absorption of FAD or energy transfer from the antenna chromophore [37].

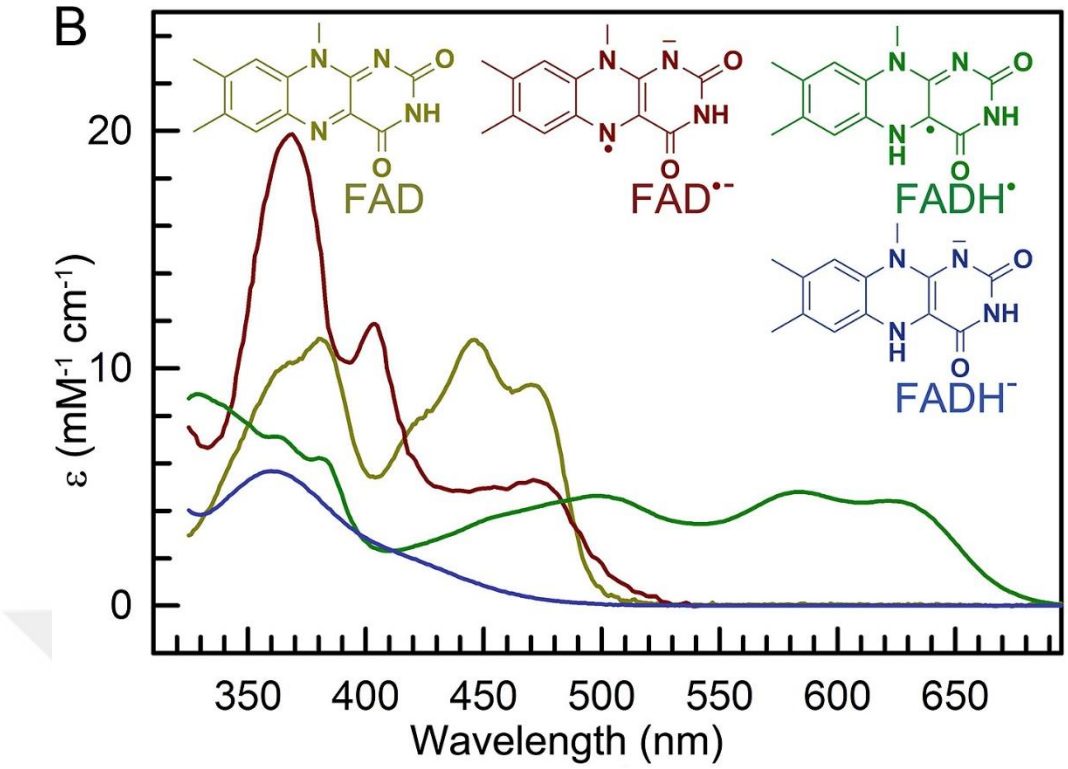

Figure 2.5: Absorption spectrum of FAD in different redox states. Reprinted from reference [38] with permission.

Photoreduction mechanism has studied heavily, and importance of tryptophan residues were suggested as important partners. *In vitro* studies have shown that, Trp306, Trp359, and Trp382 in E. coli CPD PL has initiates an electron hoping cascade. The cascade stabilizes the FAD in different redox states and required for photoreduction [39]. The essential function of Trp306 has been shown where mutated photolyase was unable to do photoreduction [40]. However, in later years, it has been shown that, the suggested pathway is not essential for photolyases *in vivo* as mutated Trp306 reside has same repair rate with the wild type photolyase in *E. coli* [41].

Another possible FAD reduction is by the help of antenna chromophore. MTHF antenna chromophore has a higher excitation coefficient and can transfer its energy to the FAD by FRET. The distance between the two cofactor is around 16 Å, which is close enough to transfer energy by long range dipole-dipole interaction [3]. The electron transfer efficiency has drastic difference between species for example *E. coli* photolyase has 69% efficiency, while *Anacystis nidulans* photolyase has up to 98% efficiency [42], [43].

2.2.9 Repair mechanism of photolyases

Photolyases specifically recognize substrate's structure and bind the lesions regardless of its sequence [44]. The DNA lesion interacts with positively charged surface residues around α-helical domain that leads to catalytic cofactor FAD [45]. Upon binding, ionic interactions between DNA-photolyase occurs while photoproduct is flipped out towards FAD [46]. The electron transfer occurs between $FADH^-$ and the DNA lesion with the help of van der Waals interactions.

Main repair steps of CPD photolyase can be seen in **Figure 2.6**. Shortly, first, forward electron transfer occurs between $FADH^{-\cdot}$ and CPD lesion, which takes 250 ps. In less than 10 ps, C5-C5'bond split that continues with either no repair back electron transfers back to $FADH^{\cdot}$, or splitting continuous with C6-C6' bond that results with repairment [47]. Overall, the repairment of CPD photolyase has around 0.82 quantum yield [47].

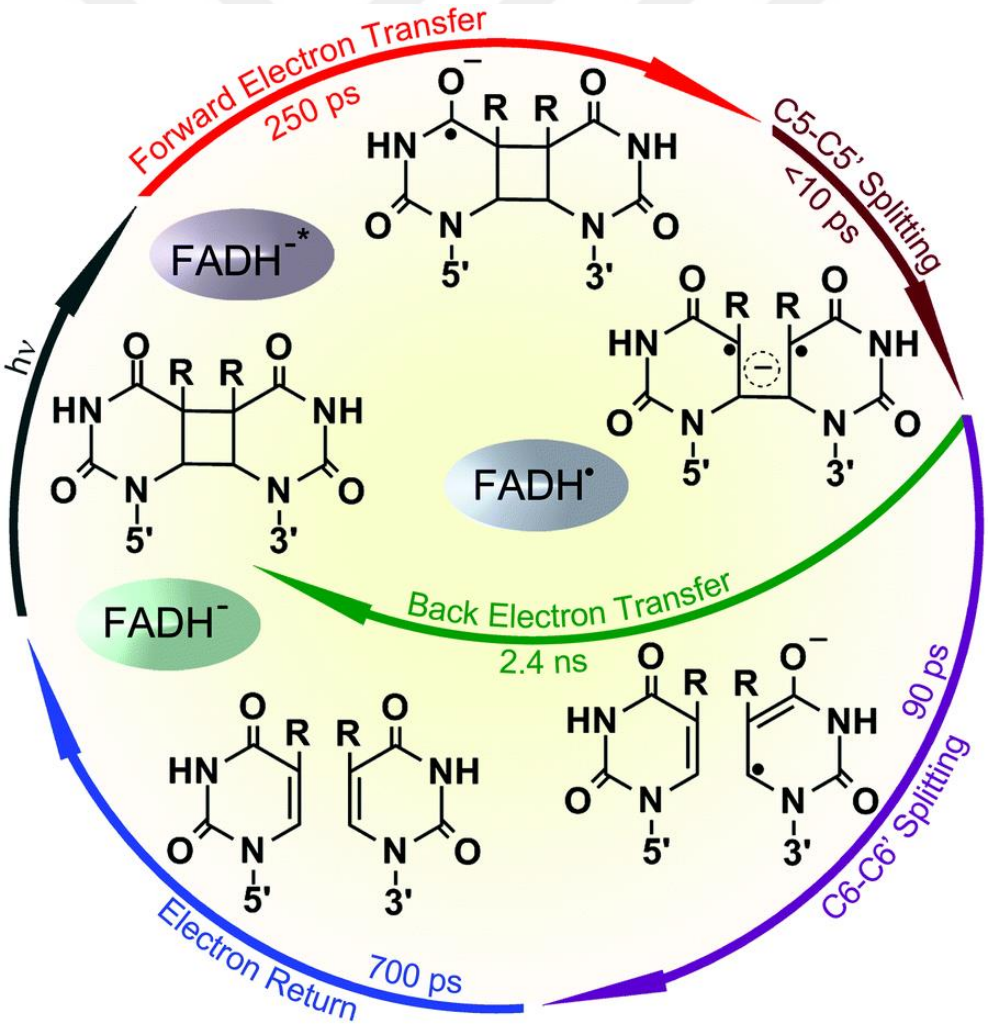

Figure 2.6: CPD repair mechanism. Reprinted from reference [47] with permission.

Unlike CPD photolyases, full repair mechanism of (6-4) photolyase is still unknown. The (6-4) PP has significantly different than CPD lesion and breaking the bond with C-C atoms is not enough to repair the damage. A functional group change has happened in (6-4) PP and it needs to be transferred back [7]. Various studies have been conducted to show the repair mechanism of the (6-4) photolyase and its working mechanism is yet to be fully revealed [48]. Main suggested mechanisms can be seen in **Figure 2.7.** Some important amino acids have been showed to be important which, some concerned some differ between eukaryote or prokaryote (6-4) photolyases. In *At*(6-4) PL, His366, Trp342, Trp390, Try391, Try399, and Tyr424 shown to be important for photoreduction/DNA binding/DNA repair [6], [49], [50]. In *Xenopus laevis*, His354, His 358, Leu355, Trp291, Trp398 are shown to be imported for the enzyme [51].

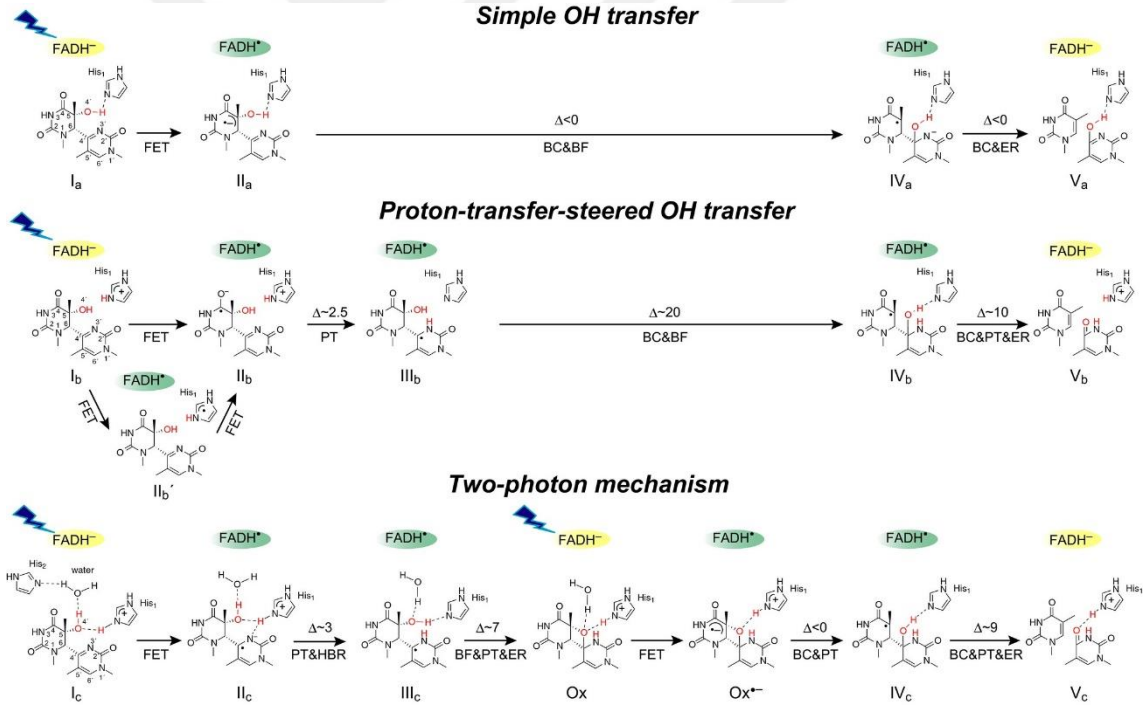

Figure 2.7: Various suggested repair mechanisms of (6-4) photolyase. Reprinted from reference [52] with permission.

2.3 Vibrio cholerae

Vibrio cholerae (O1 bivar Tor str. N16961) is a bacterium that causes sickness on human intestine. In between host infection, it lives in the aquatic environment for long time where it is subjected to both UV light and blue light. It has a particular blue light regulatory system where transcription of 6.3% of its genes are regulated by it [53] .

4 different cryptochrome/photolyase family proteins have been identified in *Vc*. 1 CPD PHR, 1 VcPHR, 1 VcCRY1, and lastly (6-4) photolyase [54] [5]. Presence of DMRL and FAD cofactor is shown by UV-vis absorption and fluorescence spectroscopy. [4Fe-4S] cluster presence has been suggested by the computational study and its repair activity is shown by slot-blot assays [5].

Chapter 3:
MATERIALS AND METHODS

3.1 Plasmid and the gene construct

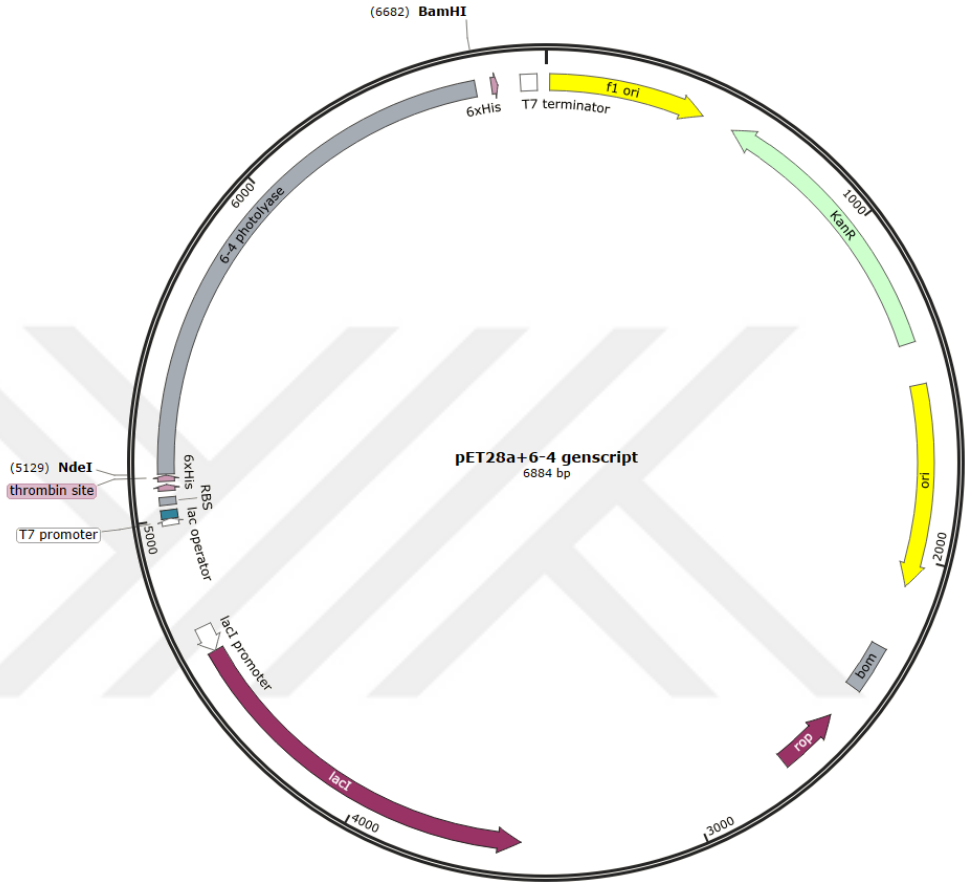

Figure 3.1: Plasmid map of pET28a(+) with (6-4) photolyase.

Full-length *(6-4) photolyase* from *Vibrio cholerae* in pET28a(+) vector between NdeI and BamHI cut sites purchased from Genscript (Piscataway, NJ, USA) as codon optimized to *Escherichia coli*. The map of the vector can be seen in **Figure 3.1**. The expressed construct from the vector is: MGSSHHHHHHSSGLVPR(thrombin cut site)GSHMRYSVVRLILGDQLNHAHSWFSEHRDDVLYLIAELHQEQEYVRHHIQ KQCAFFAAMQAFADYLSAEGHHVWHLDLDASAQYNDLPDLIAQICQQVQADA FQYQRPDEYRLLEQMANLRLSGITIGCVDTEHFLLPFAEIPEQFPASKAVLMEHF YRRMRKRFGYLMTADGKPEGGQWNFDADNRNKLKSPDLLQLPTPLCFDNPVA SIKARIERHRIPSIGQVGESLLWPINRAQALSLLAHFCQICLPNFGRFQDAMTAQ HPHRWSLYHSRLSFALNSKLLSPREVIEATISAYRAAQGQISLAQVEGFVRQILG

WREYVRGMYWSNMPHYQTRNHLGAQRPLPSYFWNGQTKMRCLQQAITQSLD FGYAHHIQRLMVTGNFALLTECDPDQVDAWYLGIYIDAIEWVELPNTRGMALF ADGGLIATKPYSASGSYINKMSDYCASCAYQVKLKSGEKACPLNSLYWRFMLK HRDRLANNPRIGMLYKTWDKMTSDSQQAILSTADAYLSQIESL*. The vector contains *kanamycin* resistance gene for selectivity and *lacI* for controlled expression of protein.

3.2 The expression and purification of (6-4) photolyase

The plasmid was transformed into *E. coli* BL21 Rosetta-2 strain and grown in 50 mL of LB-Miller with 50 µg/mL kanamycin and 35 µg/mL chloramphenicol antibiotics at 37 °C with 110 rpm shaking overnight. 0.4 mM of isopropyl β-D-thiogalactopyranoside (IPTG) is added as the final concentration. 5 and 24 hours of induced and uninduced cultures were centrifuged at 2850 g for 25 minutes at 4 °C and pellets were stored at -80 °C. Next day, 5 mL of Lysis Buffer (500 mM NaCl, 50 mM Tris-HCl pH 7.5, %5 glycerol (v/v), 0.1% Triton X-100 (v/v)) was added into pellets and sonication (Branson W250 sonifier, USA) is done at 40% power for 15 seconds at 3 times. Induced samples were centrifuged at 10000g for 10 minutes at room temperature, and 100 µL of Ni-NTA agarose resin was added to the supernatant. After 3 hours of incubation at 4 °C, centrifugation at 700 g for 2 minutes was done, and the supernatant was discarded. 1 mL of His A (200 mM NaCl, 20 mM Tris-HCl pH 7.5 (v/v)) was added to the beads, and 30 minutes of 4 °C incubation is done. Samples were recentrifuged and the supernatant was discarded. 400 µL of His B (200 mM NaCl, 20 mM Tris-HCl pH 7.5, 250 mM imidazole) was added to the beads, after 2 minutes of mixing, centrifugation is done at 700 g for 5 minutes. The supernatant was taken and applied to the 12% SDS-PAGE with all other samples.

Inoculation of *(6-4) photolyase* vector containing Rosetta-2 cell line was done into 150 mL of kanamycin and chloramphenicol containing LB Miller and incubated overnight at 37°C with 110 rpm. The culture was equally distributed into 3 1.5 L of LB with required antibiotics and conditioned incubation. When OD_{600} reached 0.8, induction was done with 0.4 mM of IPTG as the final concentration, and induction was done at 18 °C for 24h. The culture was centrifuged at 2850 g for 45 minutes at 4 °C and the pellet was stored at -80 °C for 24 h. Lysis buffer (500 mM NaCl, 50 mM Tris-HCl pH 7.5, %10 glycerol (v/v), 0.1% Triton X-100 (v/v)) was added to the pellets and sonication (Branson

W250 sonifier, USA) was done at 45 sec at 60% power 3 times. The samples were ultracentrifuged at 35000 rpm with Ti-45 rotor (Beckman, USA) for 1 hour at 4°C, then the supernatant was filtered with 45 μm cellulose mixed ester filter (ISOLAB, Germany), then applied to the Ni-NTA agarose resin (QIAGEN, USA). The column was equilibrated with His A buffer (200 mM NaCl, 20 mM Tris-HCl pH 7.5 (v/v), 5% glycerol (v/v)) then the sample was loaded with 2.5 ml/min speed. Washing of the column was done with His A, and the protein was eluted with His B Buffer (200 mM NaCl, 20 mM Tris-HCl pH 7.5, 250 mM imidazole, 5% glycerol (v/v)) into 100% glycerol to prevent precipitation of protein. Yellow colored (6-4) photolyase was quickly frozen with liquid nitrogen and stored at -80 °C with the final concentration of 25% glycerol (v/v).

3.3 Crystallization, Data collection and Processing

Crystallization was done with 5 mg/mL final concentration of (6-4) photolyase with the sitting drop, microbatch screening (under oil) method at 4 °C by mixing 0.83 μL of protein with 0.83 μL of crystal screening conditions in 72 well teresaki plates. The mixture was covered with 16.6 μL of parafilm oil to allow slow evaporation of solvents. Around 3500 commercially available crystal screening conditions were tested, and the yellow-colored crystals were observed at Wizard Synergy-I #40 (Rigaku, Japan), which contains 2 M of Ammonium citrate/citric acid pH 7.5 and 5% PEG 400 (v/v) after 7 weeks. The condition was further improved by mixing 0.5 μL Cryo-Pro #45 (Hampton research, USA), which contains 1 M Sodium Sulfate decahydrate, 1 μL of protein, 1 μL of Wizard Synergy #40. The crystals were flash frozen with liquid nitrogen, and data collection was done at 100 K. X-ray diffraction data were collected to 2.0 Å and 2.5 Å resolutions with a wavelength of 1.54 Å at University of Health Sciences (Istanbul, Turkey) with Rigaku's XtaLAB Synergy Flow X-ray diffractometer (Rigaku, Japan). X-ray generator PhotonJet-R (Rigaku, Japan) was operated at 40 kV and 30 mA with 23% beam intensity. HyPix-Arc-150° detector (Rigaku, Japan) was used with 60 mm detector distance, 1-degree scan width, and 15- and 30-sec exposure times. The total run time for the data collection was 1 h 11 min 30 sec, and 2 h 33 min 0 sec. Profit merge was done by using the data from both crystals and data reduction was done with CrysAlis Pro (2) software version 171.42.51a. Unit cell dimensions were a=200.751 Å b=200.751 Å c=77.0231 Å α=90 β=90 γ=120, the space group was $P6_4$ 2 2.

3.4 Structure Determination and Refinement

Swiss model [55], [56] was used for building a model for structure determination that gave the result with PDB ID: 4DJA [31], which was used in the automated molecular replacement program PHASER [57] in PHENIX [58] software version 1.20.1-4487. Further refinements were done with PHENIX, and the addition of water and cofactors was done in COOT [59] software version 0.9.6. Figures were generated at PyMOL [60] Version 2.4.1. Data collection and structure determination information are summarized in **Table 3.1.**

Table 3.1: Data collection and refinement statistics

Data collection & processing		Refinement	
Space group	$P6_4$ 2 2	Resolution (Å)	24.25-2.5 (2.589-2.5)
Cell dimension		Rwork/Rfree	0.22 / 0.28 (0.28) / (0.36)
a, b, c (Å)	200.751 200.751 77.0231	Reflections used in refinement	31969 (3130)
α, β, γ (°)	90 90 120	Number of atoms	4778
Wavelength (Å)	1.54	Macromolecules	4120
R_{merge}	1.382 (3.765)	Ligands	101
CC1/2	0.95 (0.54)	Average B-factor	22.46
I/σI	5.61 (1.70)	Protein B-factor	22.31
CC*	0.988 (0.84)	Ligands B-factor	17.61
Completeness (%)	99.60 (99.97)	Solvent B-factor	24.49
Multiplicity	60.4 (60.6)	Ramachandran favored (%)	98.01
Total reflections	1935882 (189833)	Ramachandran outliers (%)	0.00
Unique reflections	32043 (3130)	RMS lengths (Å)	0.002
Wilson B factor ($Å^2$)	15.97	RMS angles (°)	0.48

Chapter 4:
RESULTS

4.1 Small scale-expression of (6-4) photolyase

The small-scale expression result of (6-4) photolyase from *Vibrio cholerae* can be seen in **Figure 4.1**. 5 hours and 24 hours induction times were tried to test the better expression yield of the protein in Rosetta-2 cell line. For both trials, in induced samples, the expected bands of (6-4) photolyase can be seen, while in uninduced samples, there is no similar band. This shows that (6-4) photolyase protein is expressed and has an affinity to Ni-NTA agarose beads. There is also some protein in the pellet however, its level was low and, therefore, neglected. The presence of 56 kDa bands in the unbound sample might indicate lower affinity to Ni-NTA beads of the protein or not enough beads are used on the assay. It is also worth mentioning that pulldown with Ni-NTA agarose beads on Rosetta-2 cell line shows non-specific bindings at around 55 kDa and 41 kDa. The bands on 41 kDa in the elution lane and 55 kDa bands in the unbound lane might be explained as non-specific bindings with low affinity to Ni-NTA resins. There are no protein bands in the wash samples either because protein concentration is too low or because washing was not enough to break the low affinity of non-specific proteins. The expression level of the protein was at a similar level in both temperatures however, 5 hours induced sample had more impurities than 24 hours induction sample. As a result, 24 hours of expression with 0.4 mM of IPTG at 18 °C was selected as the better expression condition.

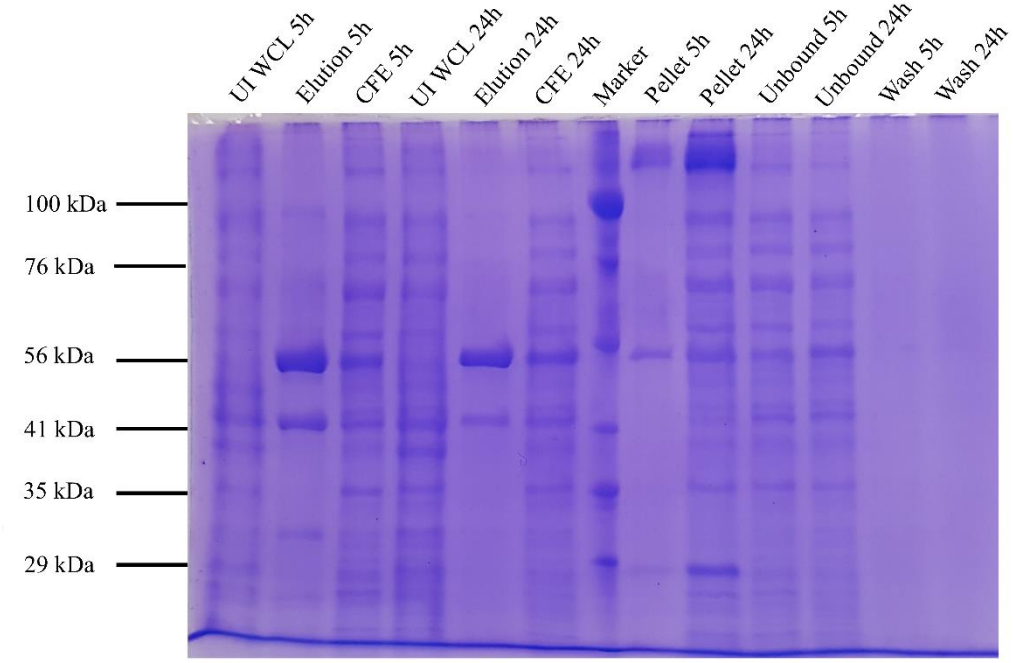

Figure 4.1: Small scale expression of (6-4) photolyase with Rosetta-2 cell line. 12% SDS-PAGE results of 5 h and 24 h induction time trials at 18°C. Unbound is the supernatant after incubation with Ni-NTA beads. Wash is the His-A buffer after the incubation with Ni-NTA beads. UI: uninduced culture, WCL: whole cell lysate, CFE: cell free extract.

4.2 Large-scale expression of (6-4) photolyase

The large-scale expression of (6-4) photolyase can be seen in **Figure 4.2A**. A small band around the ~56 kDa might be a non-specifically expressed protein or leaky expression of the (6-4) photolyase. There is some (6-4) photolyase in the pellet, although the soluble amount is still high enough to do Ni-NTA column purification. After the purification, two elution fractions are collected. Elution fraction one was 1 mg/mL with total of 25 mL while elution fraction 2 was 5 mg/mL with total of 15 mL. Both samples contained 25% glycerol to prevent precipitation of (6-4) photolyase. The samples were colored yellow due to containing FAD and DMRL, which are colorful cofactors (**Figure 4.2B**). Elution fraction 2 was darker yellow due to having a higher concentration of the enzyme and cofactors.

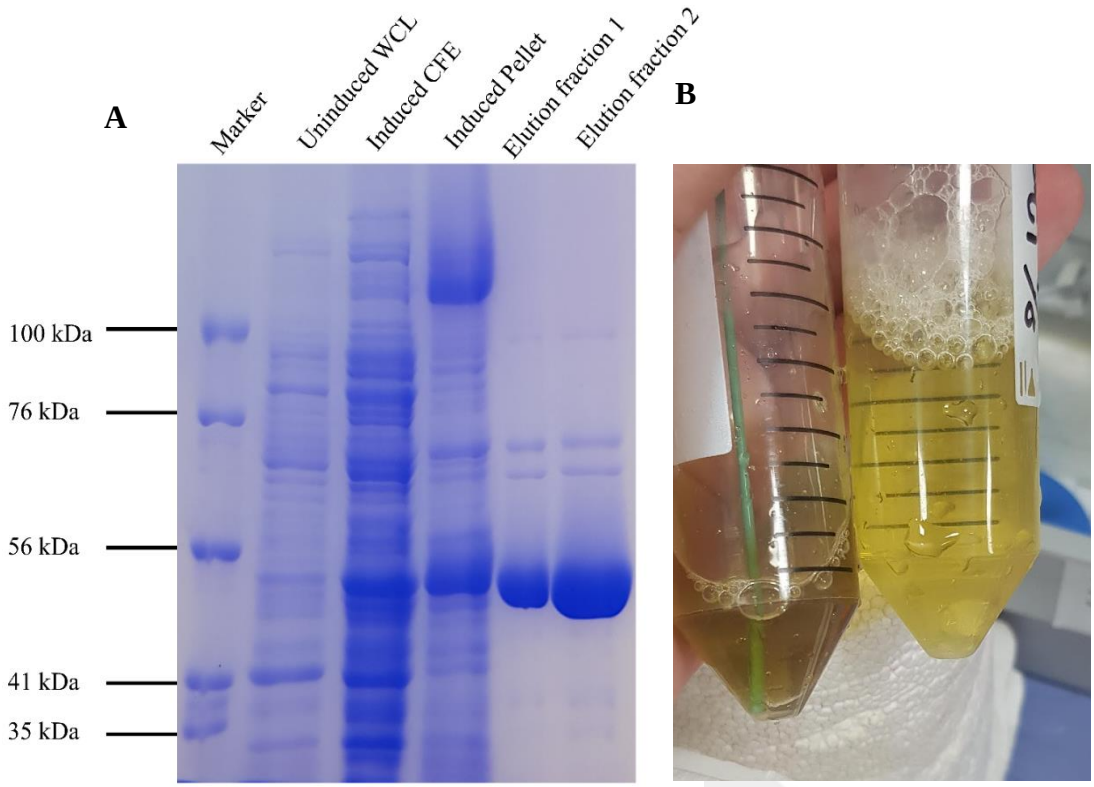

Figure 4.2: Large scale expression of (6-4) photolyase in Rosetta-2 cell line. (A) 10% SDS-PAGE results of 24 h expression at 18°C in 4.5 L. Elution fraction 1 is 1 mg/mL while elution fraction is 5 mg/mL. (B) Photography of the 2 elution fractions. Light yellow colored sample containing falcon has elution fraction 1, dark-yellow colored sample is elution fraction 2.

4.3 Crystals of (6-4) photolyase

The crystallization procedure took three days, with more than 1000 conditions being screened each day. Due to precipitation of (6-4) photolyase, crystallization continued until the aliquot of protein for the day is finished. After seven weeks of 4 °C, oval-shaped, yellow-colored crystals are formed in Wizard synergy-I #40 condition (**Figure 4.3A**). To test their content, crystals were poked via a tool, and easily destroyed, indicating their protein content. Optimizations of the condition were also done via ~150 additive screens, and different crystals formations can be seen in **Figure 4.3B,C, and D**. The largest crystals were in Cryo-Pro #45 condition however, all the crystals were sent to XRD.

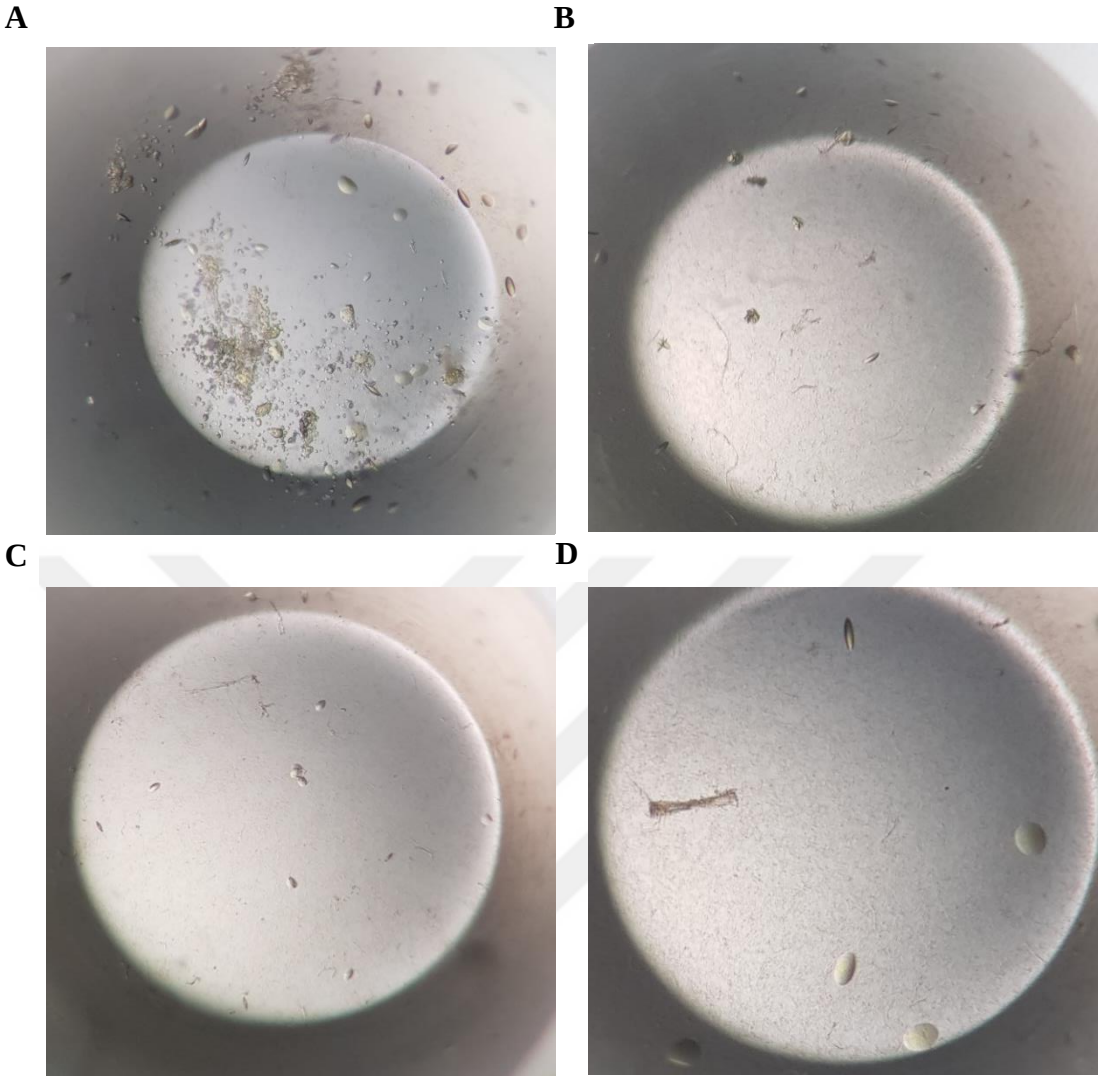

Figure 4.3: Crystals of (6-4) photolyase in terasaki plates. (A) First formed crystals in Wiz synergy-I #40 that contains 5% (v/v) PEG-400 and 2 M ammonium citrate/citric acid pH 7.5. Other crystals in wells are mixture of Wiz synergy-I #40 with additional screens. (B) Additive screen-I #25 (1 M sodium malonate pH 7.0), (C) Additive screen-II #3 (30% w/v dextran sulfate sodium salt), (D) CryoPro #45 (1 M sodium sulfate decahydrate)

4.4 Data Collection from (6-4) photolyase crystals

On XRD, the first crystals from the original Wizard synergy-I were tested. The crystals' diffraction was extremely weak, and the protein diffraction pattern was hard to see. In **Figure 4.4A**, the diffraction pattern of the best candidate can be seen. Complete data set collection is done to the best candidate crystal in cryogenic conditions, unfortunately, from this data alone, resolving the crystal structure of the protein was not possible.

When the crystals from the optimized conditions were used for data collection in XRD, most of them did not give diffraction. There were two crystals in the CryoPro #45, which gave a better diffraction pattern. Full data set collection is done to both crystals at cryogenic temperature. **In Figure 4.4B**, the best diffraction pattern from one of the crystals can be seen. Although glycerol was present in the protein, an ice ring was still formed, which lowered the resolution of data.

A **B**

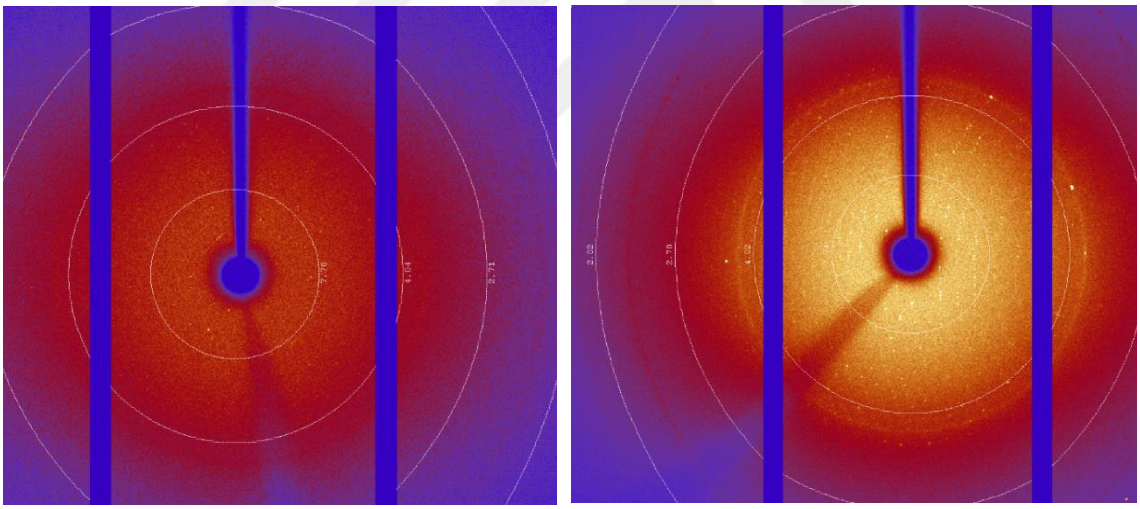

Figure 4.4: Representative X-ray diffraction pattern of (6-4) photolyase crystals. The white circles are resolution rings on the diffraction image (A) Weak diffraction pattern of crystals from Wiz synergy-I #40. (B) Stronger diffraction pattern of crystals from Wiz synergy-I #40 and CryoPro #45. A slight ring close to 4.00 Å resolution ring is an ice ring.

4.5 Structure determination and Refinement

For two crystal data sets, in one, the resolution was going up to 2 Å, while for the other, 2.5 Å was the limit. However, at high resolution on the 2 Å data set, the structure has high R_{work}/R_{free} and generally gave a bad fit in the protein structure. Refining the 2.5 Å data set gave better results however, R_{work} was never less than 25%, and Ramachandran outliers were 1%. Merging two diffraction data by profit merge of CrysAlisPro, gave a much better fitting electron cloud to the protein and lowered the R_{work} around 22%. Structure determination and refinement are continued with the merged set, and all the analysis is done according to the pdb refined by the merged electron cloud. The final R_{work} is 22.54% and R_{free} is as 28.30%, completeness is 99.60% with 24.250 to 2.500 Å refinement resolution. The structure contains 0.00% Ramachandran outliers with 98.01% favored residues.

4.6 Crystal structure of (6-4) photolyase

We recently identified a (6-4) PL from *Vibrio cholerae* (*Vc*) which possess catalytic cofactor FAD, an antenna chromophore DMRL, and additional cofactor [4Fe-4S] cluster [61]. We determined the crystal structure of *Vc*(6-4) PL at 2.5 Å resolution at cryogenic temperature. The structure contains all the cofactors with electron clouds and contains a total of 24 α helixes and 5 β sheets (**Figure 4.5A**). It consists of two domains: an α-helical domains associated with FAD and α/β domain with DMRL cofactors. The sequence alignment of *Vc*(6-4) PL with structurally available bacterial (6-4) PL with 38.4% sequence similarity with *Agrobacterium tumefaciens* (*At)*(6-4) PL and 43.1% sequence similarity with *Rhodobacter sphaeroides* **(***Rs)*(6-4) PL (**Figure 4.5B**).

A

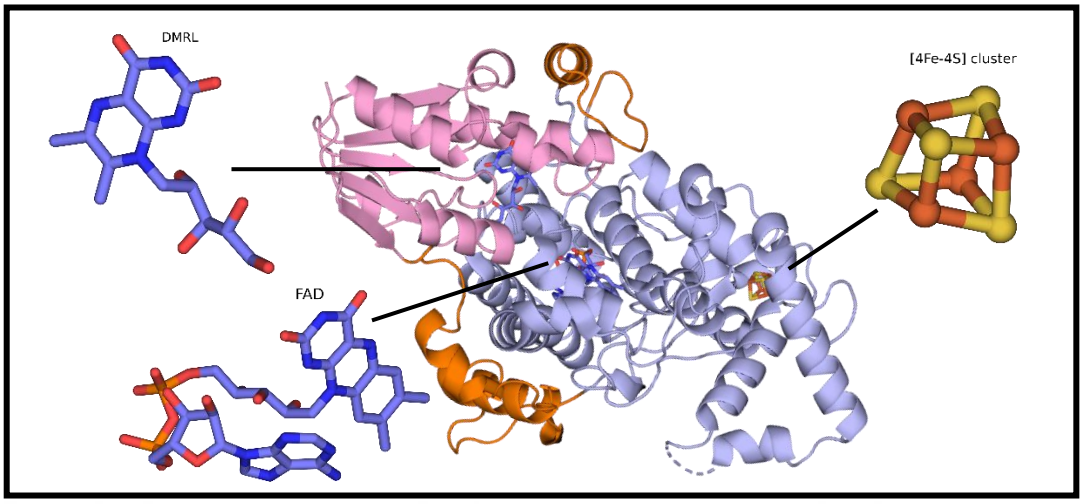

B

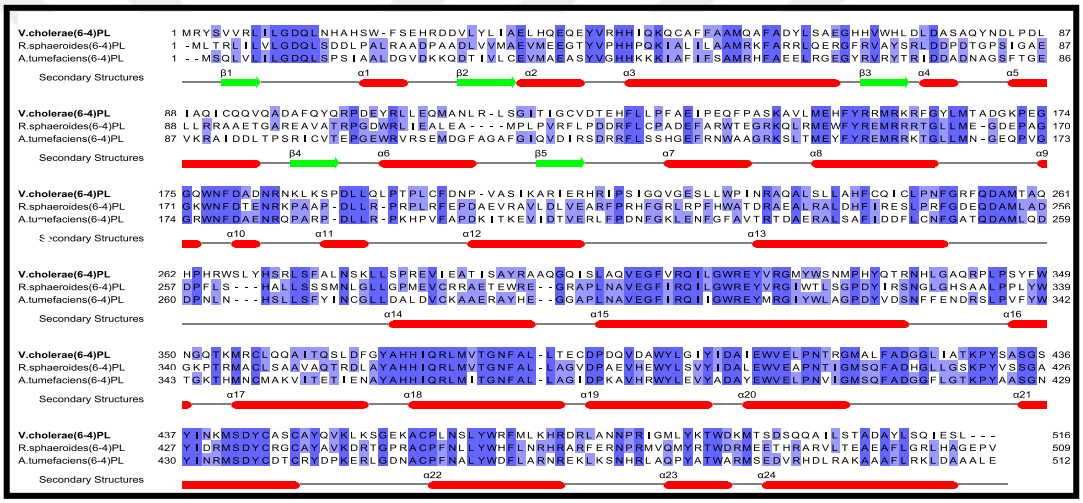

Figure 4.5: Crystal structure and sequence comparison of *Vc*(6-4) PL. (A) Overview of *Vc*(6-4) PL structure, pink is α/β-domain, light blue is catalytic domain, and orange is the inter-domain linker region. Cofactor places are indicated by the black line. (B) Sequence alignment of bacterial (6-4) photolyases with available crystal structures and secondary structures of *Vc*(6-4) PL are shown. Red lines are α helixes and green lines are β sheets. Percentage identity coloring is used in Jalview software.

4.7 DMRL Binding domain

DMRL is a photoantenna chromophore and has higher efficiency to absorb light then FAD for increasing the catalytic efficiency [31]. In the crystal structure, there is a very well-defined electron cloud of the DMRL and interacting amino acid residues (**Figure 4.6A**). Aromatic ring of DMRL interacts with nitrogen atoms of Gln11, Leu35, Gln39, and oxygen atom of Ala33 (**Figure 4.6B**). Additionally, aromatic ring of DMRL interacts with Trp488, Ala33 and Ile9. The Ribity group of the DMRL forms hydrogen bonds with oxygen of the Glu38, Tyr41, Asp12 and with amino group of Asp10. When we compare the interaction partners of DMRL in *Vc*(6-4) PL with other known bacterial (6-4) PLs, almost all the interactions are conserved with a few exceptions. First, *At*(6-4) PL, Cys32 carboxyl group interacts with aromatic ring in DMRL (PDB ID: 4DJA) while in both *Vc* and *Rs* (6-4) PLs DMRL interact with carboxyl group of Ala33. We identified a water molecule that interact with Asp12, Gln13, Asp106, and DMRL in *Vc*(6-4) PL (**Figure 4.6C**). Analyses of other bacterial (6-4) PLs have shown similar conserved motifs (**Figure 4.6C**). Such motif increases the overall stability of the DMRL within the enzyme. However, W22 molecule interacts with Asp106 of the *Vc*(6-4) PL with a distance of 2.8 Å while same interaction occurs with Gly105 of other bacterial (6-4) PLs with a distance of over 3.3 Å. These difference might increase the affinity of DMRL with *Vc*(6-4) PL.

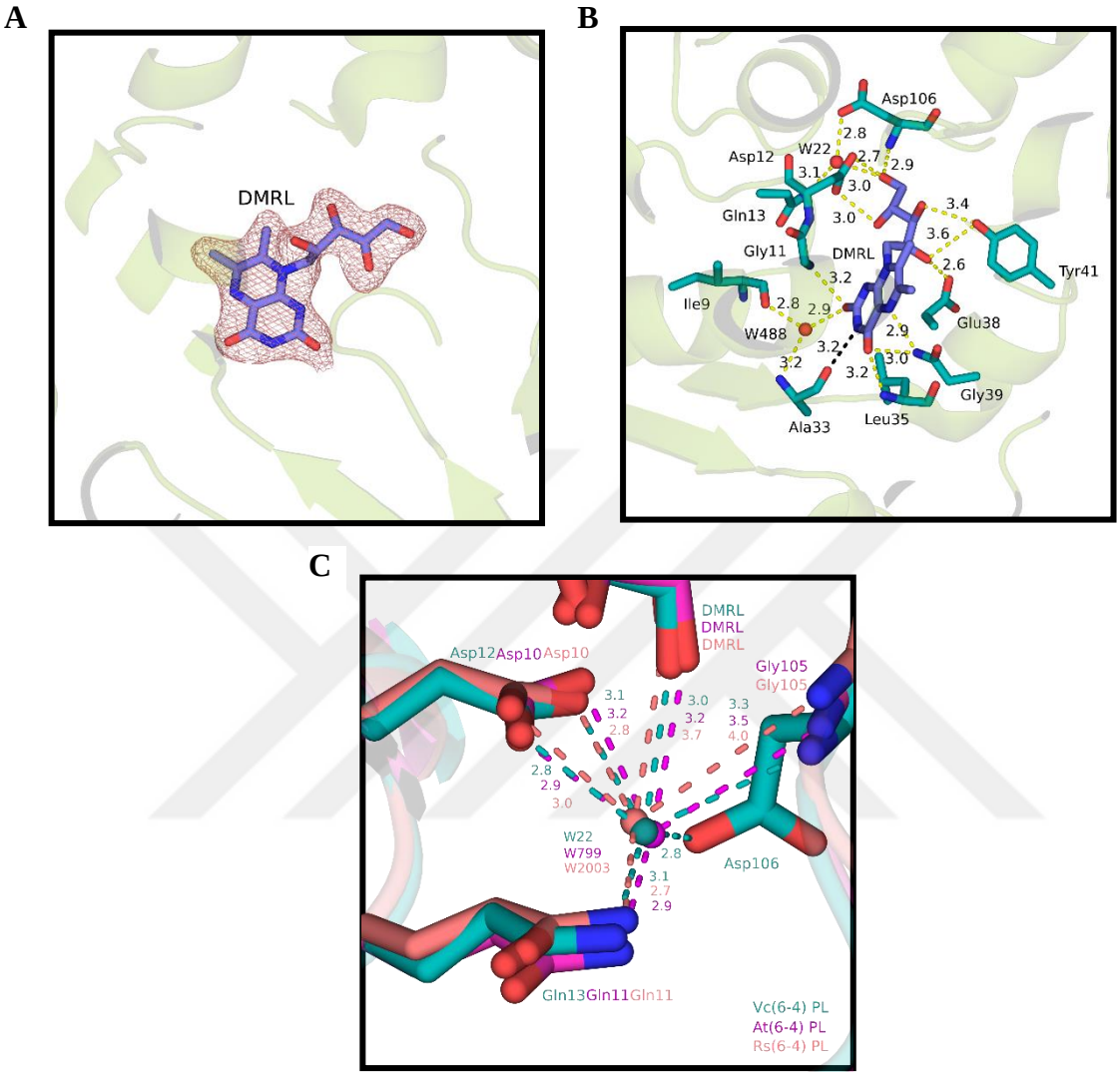

Figure 4.6: DMRL interactions and comparisons with other (6-4) photolyases. (A) Electron cloud of DMRL at σ_A-weighted 2 F_0-F_c electron density map contoured at 1.0σ in deepsalmon mesh and *Vc*(6-4) PL cartoon in splitpea color. (B) Possible interaction partners of DMRL. Yellow dashes represent hydrogen bondings, black dashes indicate Van der Waals interactions, and red dots are water molecules. (C) Additional water molecule that might stabilize the DMRL interaction. Deepteal, magenta, and deepsalmon colors indicate *Vc*(6-4) PL, *At*(6-4) PL (PDB ID: 4DJA) and *Rs*(6-4) PL (PDB ID: 3ZXS) respectively. Their superimposed structures have RMSD: 0.834 Å (*At*(6-4) PL), and RMSD: 0.876 Å (*Rs*(6-4) PL). Each dashed line represents hydrogen bonding of species with corresponding color.

4.8 FAD binding domain

FAD is located in the α-helical domain with U shaped conformation (**Figure 4.7A**). The N5 and O4 of FAD make hydrogen bonds with W7 and additional hydrogen bonds with carbonyl group of Tyr398 and NH1 side chain of Arg376 (**Figure 4.7B**). As suggested previously for other PLs [5], these interaction may also serves a stabilization function *Vc*(6-4) PL. Unlike *At*(6-4) PL or *Rs*(6-4) PL, *Vc*(6-4) PL Glu410 amino acid faces away from FAD and interacts with Asp395 rather than an His residue (**Figure 4.7B**). This results a much-relaxed interaction between the residues due to hydrogen bonding formation rather than a salt bridge formation in *Vc*(6-4) PL.

Although reaction mechanism of the CPD photolyases is elucidated, (6-4) PLs not yet fully characterized. There are different mechanisms are proposed for the (6–4) PL mechanism during DNA repair [3], [38], [62], [63]. In fact, mutagenesis studies with *Dm* (6-4) PL indicated that replacement of His365 to Asn365 result in loss of its DNA repair activity while mutagenesis of His369 into Met369 result in highly reduced the activity of *Dm*(6-4) PL [30]. However, mutagenesis studies with corresponding amino acid residues in *Xenopus* (6-4) PL showed complete loss of activity [51]. Femtosecond spectroscopy and site-directed mutagenesis suggest initial electron transfer from excited flavin induces transfer of a proton from a histidine on the active site of the enzyme to the (6–4) photoproduct [3], [64].

Catalytically active His373 (corresponds His365 of the *Dm*(6-4) PL) is conserved in *Vc*(6-4) PL (**Figure 4.7C**). In addition other conserved amino acid residues in the motif, His372 and Arg376 (corresponds to His364 and Arg368 of the *Dm*(6-4) PL) are conserved in *Vc*(6-4) PL (**Figure 4.7C**). However, the conformation of the *Vc*(6-4) PL His372 is quite different than the *Dm*(6-4) PL His364, which may indicate a different function of the residue.

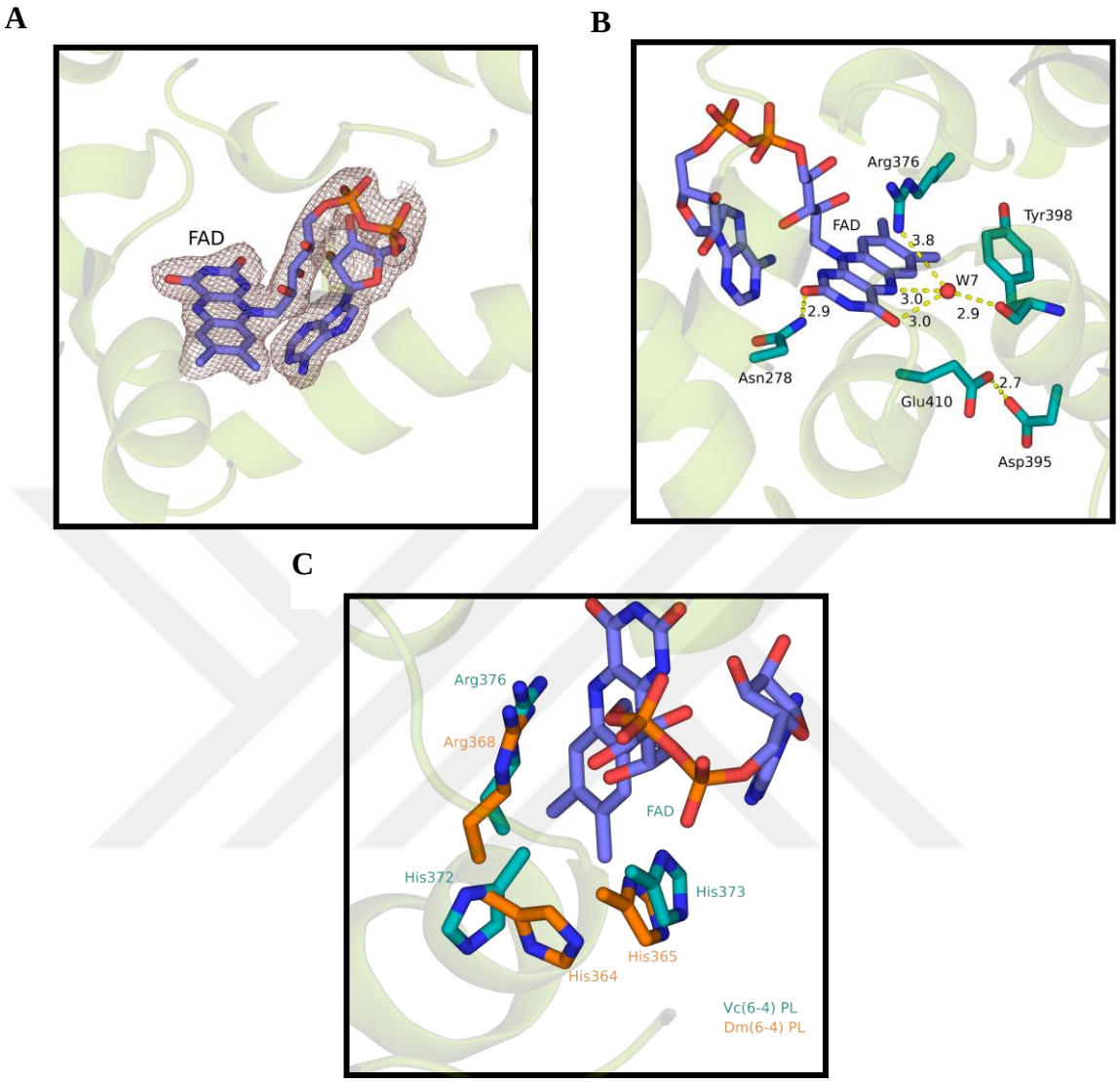

Figure 4.7: FAD interactions and comparisons with other (6-4) photolyases. Every distance is in units of Armstrong (Å). (A) Electron cloud of FAD at σ_A-weighted 2 F_0-F_c electron density map contoured at 1.0σ in deepsalmon mesh, and *Vc*(6-4) PL cartoon in splitpea color. (B) Possible interaction partners of FAD. Yellow dashes represent hydrogen bondings, red dot is a water molecule. (C) Superimposed structure of *Vc*(6-4) PL and *Dm*(6-4) PL (PDB ID: 7AYV) at RMSD: 4.350 Å. Teal color represents *Vc*(6-4) PL and tv_orange color represents *Dm(*6-4) PL.

4.9 [4Fe-4S] cluster

The structure contains an iron-sulfur cluster with an unknown function with a well-defined electron cloud (**Figure 4.8A**). Its interactions with the surrounding cytosine amino acids summarized in **Figure 4.8B**. Cys357, Cys445, Cys448, Cys461 sulfide atoms make bonds with Fe atoms in the cluster with each bond at 2.3 Å distance. The function of [4Fe-4S] cluster is currently unknown however, its distance to the FAD is 17Å, which indicates it does not have a functional activity in the DNA repair due to its distance to the catalytic region.

[4Fe-4S] clusters are known for their oxygen sensitivity, and under aerobic conditions it decomposes into [3Fe-4S] cluster and can further dissociates into [2Fe-2S]. Mostly the decomposition of the cluster deactivates the cluster containing enzymes and works require using glovebox to prevent decomposition of the [4Fe-4S] clusters. In case of *Vc*(6-4) PL, whole expression, purification, and crystallization procedures were done in atmospheric conditions that took months. In the structure, there was no damage in the [4Fe-4S] cluster, which might indicate the cluster in the photolyase is more resistant to the oxygen.

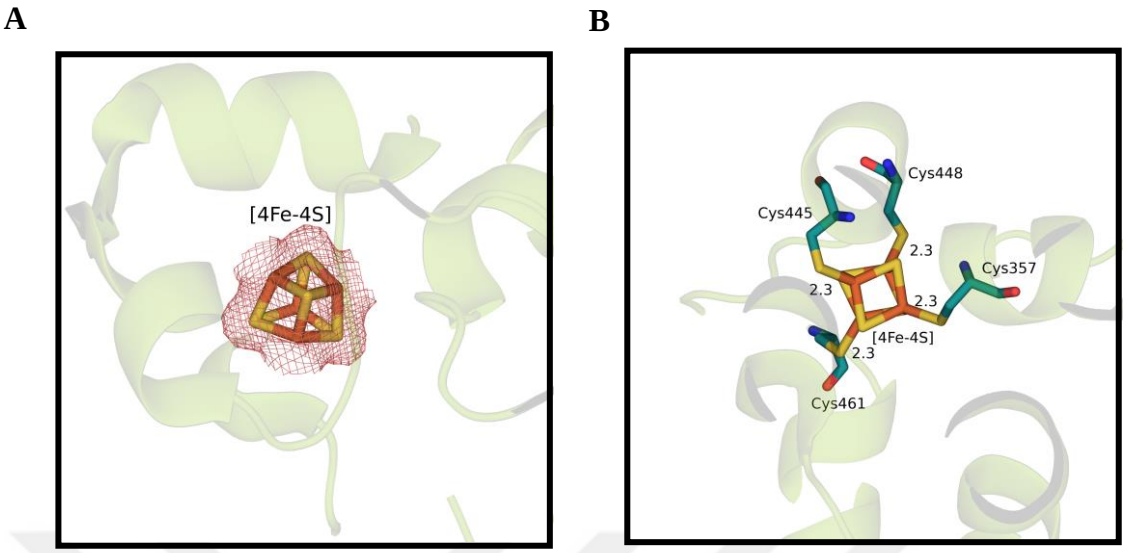

Figure 4.8: [4Fe-4S] cluster interactions. (A) Electron cloud of [4Fe-4S] cluster at σ_A-weighted 2 F_0-F_c electron density map contoured at 1.0σ in deepsalmon mesh and *Vc*(6-4) PL cartoon in splitpea color. (B) Direct interactions of [4Fe-4S] cluster with surrounding amino acids of *Vc*(6-4) PL. Every distance is in units of Armstrong (Å).

The DNA binding region of the *Vc*(6-4) PL has defined electron clouds consists of amino acids Asn178, Phe179, Asp180, Ala181, Asp182, Asn183, Arg184, and Asn185 (**Figure 4.9A**). This region has not a defined electron clouds in *At*(6-4) PL structures obtained in either cryogenic (PDB ID:4DJA) or ambient (PDB ID:6DD6) conditions (**Figure 4.9B** and **C**). A similar analysis were carried out with *Rs*(6-4) PL, where there is a well-defined electron cloud in the same region (**Figure 4.9D**). These results suggest that this region is highly stable in *Rs*(6-4) PL and *Vc*(6-4) PL but not in *At*(6-4) PL and, therefore this region has species specific stability differences.

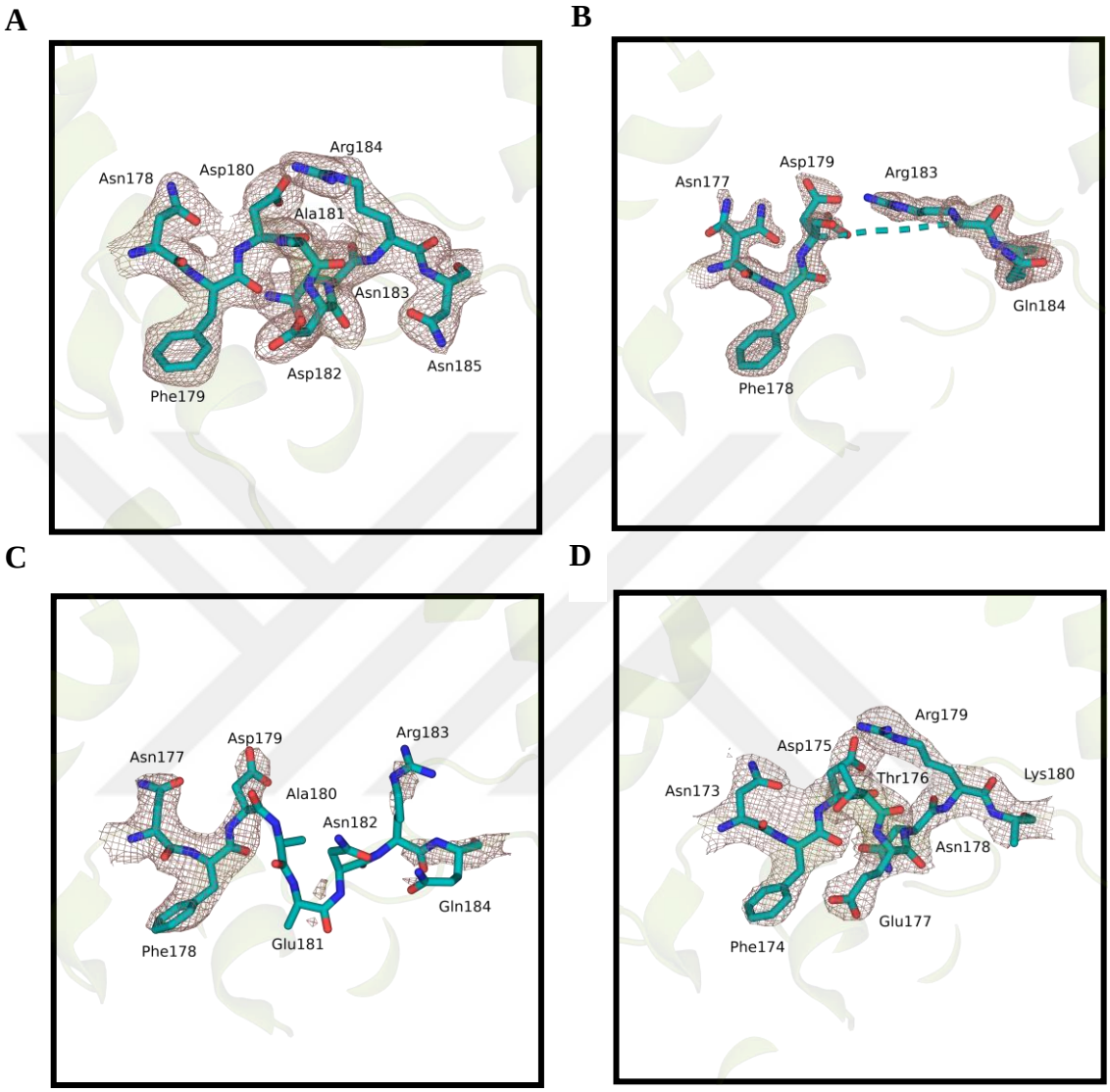

Figure 4.9: Possible DNA binding site comparison with structurally known wildtype bacterial (6-4) photolyases. Possible DNA binding sites are drawn with electron cloud at σ_A-weighted 2 F_0-F_c electron density map contoured at 1.0σ in deepsalmon mesh and (6-4) photolyase cartoon in splitpea color. (A) *Vc*(6-4) PL, (B) *At*(6-4) PL cryogenic (PDB ID: 4DJA), (C) *At*(6-4) PL ambient (PDB ID: 6DD6), (D) *Rs*(6-4) PL (PDB ID: 3ZXS). In (B), 3 amino acids are missing, which are Ala180, Glu181, Asn182, due to lack of electron cloud.

Notably, we have not observed a distinct electron cloud amino acid between 478 and 485 *Vc*(6-4) PL (**Figure 4.10A**). However, this region is distinct structures in other bacterial PLs (**Figure 4.10 B,C and D**). Interestingly, this region is adjacent to the 23rd helix, which is one of the positively surface charge helices around the catalytic region (**Figure 4.11A**). When we superimposed *Vc*(6-4) PL with *Dm*(6-4) PL (PDB ID: 3CVU) with (6-4) T-T, this region and 23rd helix were seen to pass through damaged DNA (**Figure 4.11B**). This observation suggest that region between 478 and 485 *Vc*(6-4) PL might be DNA binding region and stabilizes after interacting with the DNA lesion. Upon investigation of C-terminus of *Vc*(6-4) PL and *Dm*(6-4) PL, 2 additional helixes were identified on *Vc*(6-4) PL and 23rd helix seems to be blocking the DNA lesion in superimposed structure. Further analysis of superimposed structure showed that the catalytic cofactor FADs are in similar conformation and their RMSD is 0.7 Å (**Figure 4.11C**). To DNA lesion to bind the bacterial (6-4) PL, while still interacting with the FAD, there may be a conformational change on the 23rd helix to provide a gap for DNA lesion. B-factor analysis showed that, 23rd helix has the highest b-factor value in the structure and therefore, it has highest probability to subject a conformational change (**Figure 4.11D**). According to the superimposition of DNA lesion from *Dm*(6-4) PL with *Vc*(6-4) PL, which is compatible with a prototypical photolyase-DNA binding mode, helix α23 of *Vc*(6-4) PL interacts with the DNA, while helix α24 looks away from the DNA lesion. The surface charge of helix α23 is positive, which is consistent with the role in DNA binding. The last two helixes (α23, α24) are missing in *Dm*(6-4) PL or most of the other PLs, which can indicate their regulatory activity rather than the repair activity.

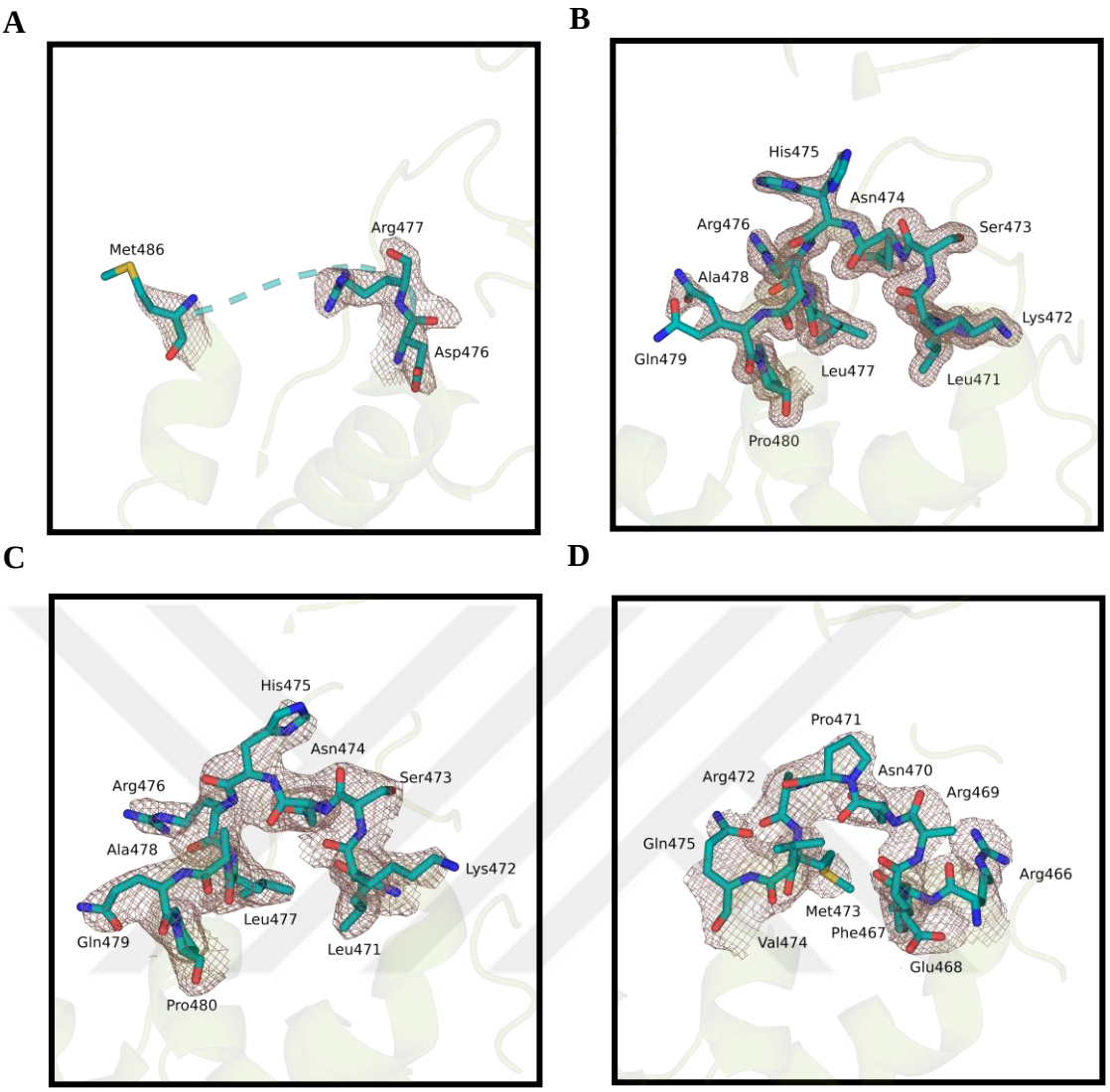

Figure 4.10: Possible DNA binding domain comparison with structurally known wildtype bacterial (6-4) photolyase. Each possible DNA binding site's electron cloud is drawn at σ_A-weighted 2 F_0-F_c electron density map contoured at 1.0σ in deepsalmon mesh and (6-4) photolyase cartoon in splitpea color. (A) *Vc*(6-4) PL, (B) *At*(6-4) PL cryogenic (PDB ID: 4DJA), (C) *At*(6-4) PL ambient (PDB ID: 6DD6), (D) *Rs*(6-4) PL (PDB ID: 3ZXS). In (A), 8 amino acids are missing, which are Leu478, Ala479, Asn480, Asn481, Pro482, Arg483, Ile484, Gly485 due to lack of electron density cloud.

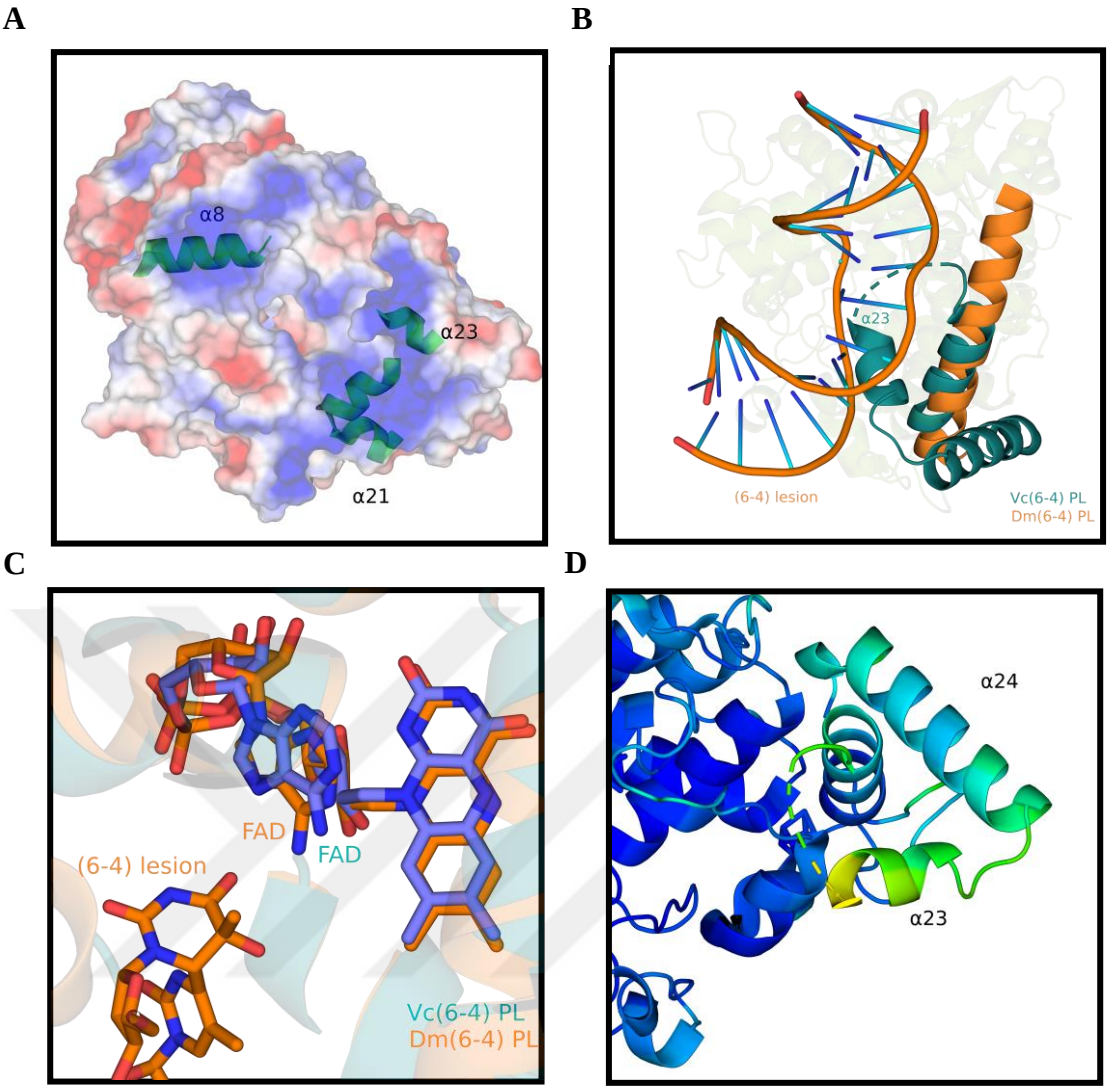

Figure 4.11: DNA binding comparison between *Vc*(6-4) PL and *Dm*(6-4) PL. (A) Generated surface density charge of *Vc*(6-4) PL, where blue is positive while red is negatively charged. Helixes with positive surface charge are indicated in the structure. (B) Superimposed (RMSD: 3.944 Å) image of *Vc*(6-4) PL and *Dm*(6-4) PL with (6-4) DNA lesion (PDB ID: 3CVU). Deepteal is for *Vc*(6-4) PL, while Tv_orange is for *Dm*(6-4) PL. (C) FAD comparison with superimposed image of *Vc*(6-4) PL and *Dm*(6-4) PL. All atoms RMSD between the structures for FAD cofactor is 0.7 Å. (D) B-factor analysis of C terminal of *Vc*(6-4) PL, where highest b-factor has yellowish color, while lowest b-factor has darker blue color. α23 has the highest b-factor in the structure.

Chapter 5:

DISCUSSION

Photolyases (PLs) belong to a large family of Cryptochrome/Photolyase responsible for repairing the UV-induced DNA damages. Different types of photolyases have been discovered [65] and they are shown to be repair two different types of DNA damages: cyclobutane pyrimidine dimers (CPD) and (6–4) PLs repair or pyrimidine-pyrimidone photoproducts photoproducts. CPD photoproducts are repaired by CPD PLs while (6-4) photoproducts are being repaired by (6-4) PLs. The reaction mechanism of CPD photolyases is elucidated at in vivo level [41], [27], [23]. On the other hand, different reaction mechanisms are proposed for the (6-4) PL. The (6-4) PLs is initially thought to specifically present in eucaryotes [31]. However, studies revealed that bacteria also possess (6-4) PLs [61],[66],[67].

Upon expression of (6-4) photolyase from *V. cholerae* in *E. coli*, a significant amount of protein is left in the pellet, which can be seen in **Figure 4.1** and **4.2**. It is known that some portions of proteins are solubilized, while the rest of them might stay in the pellet. However, the reason for such phenomenon in the case of (6-4) photolyase might be the lack of enough [4Fe-4S] cluster in the culture. When [4Fe-4S] cluster is not bound to the (6-4) photolyase, it is stuck at the pellet [6]. This might be the reason for relatively thick pellet bands in the SDS-PAGE.

On data collection at the XRD, ice ring formation was observed, formed by the liquid nitrogen's cooling environment (**Figure 4.4B**). Ice ring can prevent high resolution data collection due to giving intense bands upon diffraction as a ring and hinder any diffraction outside of the ring. Cryoprotectants are chemicals that prevent ice ring formation, and glycerol is one of the widely used cryoprotectants that prevents ice ring formation [68]. The crystal solution had glycerol in it already, therefore, additional glycerol did not use upon cryofreezing however, the ice ring is still formed. Additional glycerol could have been preventing the ice ring formation and there could have been a higher resolution structure. On the other hand, it is worth mentioning that there are different cryoprotectants and that the wrong one might damage the crystal, preventing

any data collection. There are ways to minimize the damage of ice rings to the diffraction data while the data reduction procedure, however, full damage cannot be undone [69]. Like many procedures in crystallography, trial and error is the way to choose the correct cryoprotectant however, any wrong choice might be the end of precious protein crystals.

Comparison of the crystal structure of the *Vc*(6-4) PL with other known bacterial (6-4) PLs indicated that that cofactors binding the region is well conserved with some differences: a water molecule interacts with the Asp106 in *Vc*(6-4) PL with a very short distance compare to the *At,* and *Rs* (6-4) PLs, where water molecule interacts with Gly105 (**Figure 4.6C**). The FAD binding region of the *Vc*(6-4) PL is highly conserved. However, one notable difference is that Glu410 makes a hydrogen bond with Asp395; however, in the case of Glu399 (corresponds to Glu410 of *Vc*(6-4) PL) makes a salt bridge with His384 (corresponds to Asp395 of *Vc*(6-4) PL) *At*(6-4) PL and *Rs*(6-4) PL [31], [66]. Whether such structural difference affects its activity or conformation of FAD needs to be shown. The HIS-HIS-X-X-ARG motif in (6-4) PLs is shown to be important for their catalytic activity [66]. This motif is also conserved in the *Vc*(6-4) PL. Further conformational comparison of the *Vc*(6-4) PL and *Dm*(6-4) PL of this motif indicates His373 and Arg376 of *Dm*(6-4) PL have identical configuration while His372 (His364 of *Dm*(6-4) PL) acquired a different configuration, which may reveal similar/different functionalities between species.

One of the major difference between *Vc*(6-4) PL and *At*(6-4) PL structures is their predicted DNA binding site (**Figure 4.9**). The predicted site (amino acid residues between 178 and 185) has distinct structure compared to *At*(6-4) PL, where corresponding region has no defined structure (17). The same region of *Rs*(6-4) PL has also a nice electron cloud except its Arg residues(16) .which indicates species specific stability differences of DNA binding domains. Comparison of *Vc*(6-4) PL and *At*(6-4) PL revealed that *Vc*(6-4) PL has unstructured region with 8 amino acid residues (**Figure 4.10A**), which might be DNA binding region and also conserved in other bacterial PLs. Arg483 might form a salt bridge with (6-4) photoproduct that stabilize the disordered region. The general structure of *Vc* and *Dm*(6-4) PLs are highly similar except in C terminus, where *Vc*(6-4) PLs contain additional 2 helixes. Due to position of 23rd helix, DNA lesion cannot bind the *Vc*(6-4) PL similar to *Dm*(6-4) PL (**Figure 4.11B**). However, the FADs are located extremely similar manner, which indicates a similar DNA lesion binding between the PLs

(**Figure 4.11C**). A conformational change upon DNA binding at the *Vc*(6-4) PL might open a space for DNA to bind. The 23rd helix is the main candidate for the conformational change as it is the major blocker of the DNA and has the largest b-factor (**Figure 4.11D**).

BIBLIOGRAPHY

[1] R. P. Sinha and D. P. Häder, "UV-induced DNA damage and repair: A review," *Photochemical and Photobiological Sciences*, vol. 1, no. 4, pp. 225–236, Apr. 2002, doi: 10.1039/B201230H.

[2] N. Ozturk, "Phylogenetic and Functional Classification of the Photolyase/Cryptochrome Family," *Photochemistry and Photobiology*, vol. 93, no. 1, pp. 104–111, Jan. 2017, doi: 10.1111/PHP.12676.

[3] D. Zhong, "Electron Transfer Mechanisms of DNA Repair by Photolyase," *http://dx.doi.org/10.1146/annurev-physchem-040513-103631*, vol. 66, pp. 691–715, Apr. 2015, doi: 10.1146/ANNUREV-PHYSCHEM-040513-103631.

[4] I. H. Kavakli *et al.*, "The Photolyase/Cryptochrome Family of Proteins as DNA Repair Enzymes and Transcriptional Repressors," *Photochemistry and Photobiology*, vol. 93, no. 1, pp. 93–103, Jan. 2017, doi: 10.1111/PHP.12669.

[5] U. M. Dikbas *et al.*, "Identification and Characterization of a New Class of (6−4) Photolyase from Vibrio cholerae," 2019, doi: 10.1021/acs.biochem.9b00766.

[6] D. Graf *et al.*, "Key amino acids in the bacterial (6-4) photolyase PhrB from Agrobacterium fabrum," *PLoS ONE*, vol. 10, no. 10, Oct. 2015, doi: 10.1371/journal.pone.0140955.

[7] R. P. Rastogi, Richa, A. Kumar, M. B. Tyagi, and R. P. Sinha, "Molecular Mechanisms of Ultraviolet Radiation-Induced DNA Damage and Repair," *Journal of Nucleic Acids*, vol. 2010, 2010, doi: 10.4061/2010/592980.

[8] A. Sancar, "Structure and Function of DNA Photolyase and Cryptochrome Blue-Light Photoreceptors," 2003, doi: 10.1021/cr0204348.

[9] R. P. Rastogi, A. Kumar, M. B. Tyagi, and R. P. Sinha, "Access to," *Research Journal of Nucleic Acids*, vol. 2010, p. 32, 2010, doi: 10.4061/2010/592980.

[10] E. Schäfer and F. Nagy, "Photomorphogenesis in plants and bacteria," *Photomorphogenesis in Plants and Bacteria*, pp. 1–662, 2006, doi: 10.1007/1-4020-3811-9.

[11] C. Lin, "Blue Light Receptors and Signal Transduction," *The Plant Cell*, vol. 14, no. Suppl, p. s207, 2002, doi: 10.1105/TPC.000646.

[12] A. Takemiya, S. I. Inoue, M. Doi, T. Kinoshita, and K. I. Shimazaki, "Phototropins Promote Plant Growth in Response to Blue Light in Low Light

Environments," *The Plant Cell*, vol. 17, no. 4, p. 1120, 2005, doi: 10.1105/TPC.104.030049.

[13] D.-P. Häder, "UV-B Impact on the Life of Aquatic Plants," *Modern Trends in Applied Aquatic Ecology*, pp. 149–172, 2003, doi: 10.1007/978-1-4615-0221-0_7.

[14] "Effect of Visible Light on the Recovery of Streptomyces griseus conidia from Ultra-Violet Irradiation Injury on JSTOR." https://www.jstor.org/stable/88227?seq=1 (accessed Jul. 10, 2022).

[15] C. S. RUPERT, "Photoenzymatic Repair of Ultraviolet Damage in DNA I. Kinetics of the reaction," *Journal of General Physiology*, vol. 45, no. 4, pp. 703–724, Mar. 1962, doi: 10.1085/JGP.45.4.703.

[16] M. S. Jorns, E. T. Baldwin, G. B. Sancar, and A. Sancar, "Action mechanism of Escherichia coli DNA photolyase. II. Role of the chromophores in catalysis.," *Journal of Biological Chemistry*, vol. 262, no. 1, pp. 486–491, Jan. 1987, doi: 10.1016/S0021-9258(19)75953-5.

[17] C. Tan *et al.*, "Direct Determination of Resonance Energy Transfer in Photolyase: Structural Alignment for the Functional State," 2014, doi: 10.1021/jp504349b.

[18] L. O. Essen and T. Klar, "Light-driven DNA repair by photolyases," *Cellular and Molecular Life Sciences*, vol. 63, no. 11, pp. 1266–1277, Jun. 2006, doi: 10.1007/S00018-005-5447-Y.

[19] I. H. Kavakli *et al.*, "The Photolyase/Cryptochrome Family of Proteins as DNA Repair Enzymes and Transcriptional Repressors," *Photochemistry and Photobiology*, vol. 93, no. 1, pp. 93–103, Jan. 2017, doi: 10.1111/PHP.12669.

[20] F. Zhang *et al.*, "Crystal Structures of Bacterial (6-4) Photolyase Mutants with Impaired DNA Repair Activity," *Photochem Photobiol*, vol. 93, no. 1, pp. 304–314, Jan. 2017, doi: 10.1111/PHP.12699.

[21] H. W. Park, S. T. Kim, A. Sancar, and J. Deisenhofer, "Crystal Structure of DNA Photolyase from Escherichia coli," *Science (1979)*, vol. 268, no. 5219, pp. 1866–1872, 1995, doi: 10.1126/SCIENCE.7604260.

[22] A. Mees *et al.*, "Crystal structure of a photolyase bound to a CPD-like DNA lesion after in situ repair," *Science (1979)*, vol. 306, no. 5702, pp. 1789–1793, Dec. 2004, doi: 10.1126/SCIENCE.1101598.

[23] A. Sancar, “Mechanisms of DNA Repair by Photolyase and Excision Nuclease (Nobel Lecture),” *Angewandte Chemie International Edition*, vol. 55, no. 30, pp. 8502–8527, Jul. 2016, doi: 10.1002/ANIE.201601524.

[24] S. Kiontke, T. Göbel, A. Brych, and A. Batschauer, “DASH-type cryptochromes - Solved and open questions,” *Biological Chemistry*, vol. 401, no. 12, pp. 1487–1493, Nov. 2020, doi: 10.1515/HSZ-2020-0182/MACHINEREADABLECITATION/RIS.

[25] R. Brudler *et al.*, “Identification of a New Cryptochrome Class: Structure, Function, and Evolution,” *Molecular Cell*, vol. 11, no. 1, pp. 59–67, Jan. 2003, doi: 10.1016/S1097-2765(03)00008-X.

[26] C. P. Selby and A. Sancar, “A cryptochrome/photolyase class of enzymes with single-stranded DNA-specific photolyase activity,” *Proc Natl Acad Sci U S A*, vol. 103, no. 47, pp. 17696–17700, Nov. 2006, doi: 10.1073/PNAS.0607993103.

[27] I. H. Kavakli, N. Ozturk, and S. Gul, “DNA repair by photolyases,” *Adv Protein Chem Struct Biol*, vol. 115, pp. 1–19, Jan. 2019, doi: 10.1016/BS.APCSB.2018.10.003.

[28] H. Asimgil and I. H. Kavakli, “Purification and characterization of five members of photolyase/cryptochrome family from Cyanidioschyzon merolae,” *Plant Science*, vol. 185–186, pp. 190–198, Apr. 2012, doi: 10.1016/J.PLANTSCI.2011.10.005.

[29] T. Todo *et al.*, “A new photoreactivating enzyme that specifically repairs ultraviolet light-induced (6-4)photoproducts,” *Nature 1993 361:6410*, vol. 361, no. 6410, pp. 371–374, 1993, doi: 10.1038/361371a0.

[30] M. J. Maul *et al.*, “Crystal Structure and Mechanism of a DNA (6-4) Photolyase,” *Angewandte Chemie International Edition*, vol. 47, no. 52, pp. 10076–10080, Dec. 2008, doi: 10.1002/ANIE.200804268.

[31] F. Zhang, P. Scheerer, I. Oberpichler, T. Lamparter, and N. Krauß, “Crystal structure of a prokaryotic (6-4) photolyase with an Fe-S cluster and a 6,7-dimethyl-8-ribityllumazine antenna chromophore,” *Proc Natl Acad Sci U S A*, vol. 110, no. 18, pp. 7217–7222, Apr. 2013, doi: 10.1073/PNAS.1302377110/SUPPL_FILE/ST03.DOCX.

[32] M. F. White and M. S. Dillingham, “Iron–sulphur clusters in nucleic acid processing enzymes,” *Current Opinion in Structural Biology*, vol. 22, no. 1, pp. 94–100, Feb. 2012, doi: 10.1016/J.SBI.2011.11.004.

[33] A. K. Boal, E. Yavin, and J. K. Barton, “DNA repair glycosylases with a [4Fe–4S] cluster: A redox cofactor for DNA-mediated charge transport?,” *Journal of Inorganic Biochemistry*, vol. 101, no. 11–12, pp. 1913–1921, Nov. 2007, doi: 10.1016/J.JINORGBIO.2007.05.001.

[34] J. A. Imlay, “Iron-sulphur clusters and the problem with oxygen,” *Molecular Microbiology*, vol. 59, no. 4, pp. 1073–1082, Feb. 2006, doi: 10.1111/J.1365-2958.2006.05028.X.

[35] B. Liu, H. Liu, D. Zhong, and C. Lin, “Searching for a photocycle of the cryptochrome photoreceptors,” *Current Opinion in Plant Biology*, vol. 13, no. 5, pp. 578–586, Oct. 2010, doi: 10.1016/J.PBI.2010.09.005.

[36] Z. Liu *et al.*, “Dynamic determination of the functional state in photolyase and the implication for cryptochrome,” *Proc Natl Acad Sci U S A*, vol. 110, no. 32, pp. 12972–12977, Aug. 2013, doi: 10.1073/PNAS.1311077110/-/DCSUPPLEMENTAL.

[37] I. H. Kavakli *et al.*, “The Photolyase/Cryptochrome Family of Proteins as DNA Repair Enzymes and Transcriptional Repressors,” *Photochemistry and Photobiology*, vol. 93, no. 1, pp. 93–103, Jan. 2017, doi: 10.1111/PHP.12669.

[38] M. Zhang, L. Wang, and D. Zhong, “Photolyase: Dynamics and electron-transfer mechanisms of DNA repair,” *Archives of Biochemistry and Biophysics*, vol. 632, pp. 158–174, Oct. 2017, doi: 10.1016/J.ABB.2017.08.007.

[39] Z. Liu, C. Tan, X. Guo, J. Li, L. Wang, and D. Zhong, “Dynamic determination of active-site reactivity in semiquinone photolyase by the cofactor photoreduction,” *Journal of Physical Chemistry Letters*, vol. 5, no. 5, pp. 820–825, Mar. 2014, doi: 10.1021/JZ500077S/SUPPL_FILE/JZ500077S_SI_001.PDF.

[40] Y. F. Li, A. Sancar, and P. F. Heelis, “Active site of DNA photolyase: tryptophan-306 is the intrinsic hydrogen atom donor essential for flavin radical photoreduction and DNA repair in vitro,” *Biochemistry*, vol. 30, no. 25, pp. 6322–6329, Jun. 1991, doi: 10.1021/BI00239A034.

[41] I. H. Kavakli and A. Sancar, “Analysis of the role of intraprotein electron transfer in photoreactivation by DNA photolyase in vivo,” *Biochemistry*, vol. 43, no. 48, pp. 15103–15110, Dec. 2004, doi: 10.1021/BI0478796/ASSET/IMAGES/LARGE/BI0478796F00005.JPEG.

[42] G. Payne and A. Sancar, “Absolute Action Spectrum of E-FADH2 and E-FADH2-MTHF Forms of Escherichia coli DNA Photolyase,” *Biochemistry*, vol. 29, no. 33, pp. 7715–7727, Aug. 1990, doi: 10.1021/BI00485A021/ASSET/BI00485A021.FP.PNG_V03.

[43] T. Tamada *et al.*, “Crystal structure of DMA photolyase from Anacystis nidulans,” *Nature Structural Biology 1997 4:11*, vol. 4, no. 11, pp. 887–891, Nov. 1997, doi: 10.1038/nsb1197-887.

[44] S.-T. Kim and A. Sancar, “Effect of Base, Pentose, and Phosphodiester Backbone Structures on Binding and Repair of Pyrimidine Dimers by Escherichia coli DNA Photolyase,” 1991. [Online]. Available: https://pubs.acs.org/sharingguidelines

[45] A. Mees *et al.*, “Crystal structure of a photolyase bound to a CPD-like DNA lesion after in situ repair,” *Science (1979)*, vol. 306, no. 5702, pp. 1789–1793, Dec. 2004, doi: 10.1126/SCIENCE.1101598/SUPPL_FILE/MEES-SOM.PDF.

[46] H. W. Park, S. T. Kim, A. Sancar, and J. Deisenhofer, “Crystal structure of DNA photolyase from Escherichia coli,” *Science*, vol. 268, no. 5219, pp. 1866–1872, 1995, doi: 10.1126/SCIENCE.7604260.

[47] Z. Liu, L. Wang, and D. Zhong, “Dynamics and mechanisms of DNA repair by photolyase,” *Physical Chemistry Chemical Physics*, vol. 17, no. 18, pp. 11933–11949, Apr. 2015, doi: 10.1039/C4CP05286B.

[48] J. Yamamoto, P. Plaza, and K. Brettel, “Repair of (6-4) Lesions in DNA by (6-4) Photolyase: 20 Years of Quest for the Photoreaction Mechanism,” *Photochemistry and Photobiology*, vol. 93, no. 1, pp. 51–66, Jan. 2017, doi: 10.1111/PHP.12696.

[49] F. Zhang *et al.*, “Crystal Structures of Bacterial (6-4) Photolyase Mutants with Impaired DNA Repair Activity,” *Photochem Photobiol*, vol. 93, no. 1, pp. 304–314, Jan. 2017, doi: 10.1111/PHP.12699.

[50] D. Holub, H. Ma, N. Krauß, T. Lamparter, M. Elstner, and N. Gillet, “Functional role of an unusual tyrosine residue in the electron transfer chain of a prokaryotic (6–4) photolyase,” *Chemical Science*, vol. 9, no. 5, pp. 1259–1272, Jan. 2018, doi: 10.1039/C7SC03386A.

[51] K. Hitomi *et al.*, “Role of two histidines in the (6-4) photolyase reaction,” *J Biol Chem*, vol. 276, no. 13, pp. 10103–10109, Mar. 2001, doi: 10.1074/JBC.M008828200.

[52] J. Yamamoto, P. Plaza, K. Brettel, and K. B. Repair, “Lesions in DNA by (6-4) Photolyase: 20 Years of Quest for the Photoreaction Mechanism,” *Photochemistry and Photobiology*, vol. 93, no. 4, pp. 51–66, 2016, doi: 10.1111/php.12696ï.

[53] M. Tardu, S. Bulut, and I. H. Kavakli, “MerR and ChrR mediate blue light induced photo-oxidative stress response at the transcriptional level in Vibrio cholerae,” *Scientific Reports 2017 7:1*, vol. 7, no. 1, pp. 1–15, Jan. 2017, doi: 10.1038/srep40817.

[54] E. N. Worthington, I. H. Kavakli, G. Berrocal-Tito, B. E. Bondo, and A. Sancar, “Purification and Characterization of Three Members of the Photolyase/Cryptochrome Family Blue-light Photoreceptors from Vibrio cholerae,” *Journal of Biological Chemistry*, vol. 278, no. 40, pp. 39143–39154, Oct. 2003, doi: 10.1074/JBC.M305792200.

[55] A. Waterhouse *et al.*, “SWISS-MODEL: homology modelling of protein structures and complexes,” *Nucleic Acids Research*, vol. 46, no. W1, pp. W296–W303, Jul. 2018, doi: 10.1093/NAR/GKY427.

[56] S. Bienert *et al.*, “The SWISS-MODEL Repository-new features and functionality,” *Nucleic Acids Research*, vol. 45, pp. 313–319, 2016, doi: 10.1093/nar/gkw1132.

[57] A. J. McCoy, R. W. Grosse-Kunstleve, P. D. Adams, M. D. Winn, L. C. Storoni, and R. J. Read, “Phaser crystallographic software,” *urn:issn:0021-8898*, vol. 40, no. 4, pp. 658–674, Jul. 2007, doi: 10.1107/S0021889807021206.

[58] P. D. Adams *et al.*, “PHENIX: a comprehensive Python-based system for macromolecular structure solution,” *Acta Crystallogr D Biol Crystallogr*, vol. 66, no. Pt 2, pp. 213–221, 2010, doi: 10.1107/S0907444909052925.

[59] P. Emsley and K. Cowtan, “Coot: model-building tools for molecular graphics,” *Acta Crystallogr D Biol Crystallogr*, vol. 60, no. Pt 12 Pt 1, pp. 2126–2132, Dec. 2004, doi: 10.1107/S0907444904019158.

[60] “PyMOL | pymol.org.” https://pymol.org/2/ (accessed Jul. 03, 2022).

[61] U. M. Dikbas *et al.*, “Identification and Characterization of a New Class of (6-4) Photolyase from Vibrio cholerae,” *Biochemistry*, vol. 58, no. 43, pp. 4352–4360, Oct. 2019, doi: 10.1021/ACS.BIOCHEM.9B00766.

[62] T. Matsubara, N. Araida, D. Hayashi, and H. Yamada, “Computational Study on the Mechanism of the Electron-Transfer-Induced Repair of the (64) TT

Photoproduct of DNA by Photolyase: Possibility of a Radical Cation Pathway," 2014, doi: 10.1246/bcsj.20130298.

[63] S. Faraji and A. Dreuw, "Insights into Light-driven DNA Repair by Photolyases: Challenges and Opportunities for Electronic Structure Theory," *Photochemistry and Photobiology*, vol. 93, no. 1, pp. 37–50, Jan. 2017, doi: 10.1111/PHP.12679.

[64] J. Li *et al.*, "Dynamics and mechanism of repair of ultraviolet-induced (6-4) photoproduct by photolyase," *Nature*, vol. 466, no. 7308, pp. 887–890, Aug. 2010, doi: 10.1038/NATURE09192.

[65] A. Sancar, "Photolyase and cryptochrome blue-light photoreceptors," *Adv Protein Chem*, vol. 69, pp. 73–100, 2004, doi: 10.1016/S0065-3233(04)69003-6.

[66] Y. Geisselbrecht, S. Frühwirth, C. Schroeder, A. J. Pierik, G. Klug, and L. O. Essen, "CryB from Rhodobacter sphaeroides: a unique class of cryptochromes with new cofactors," *EMBO Rep*, vol. 13, no. 3, pp. 223–229, Mar. 2012, doi: 10.1038/EMBOR.2012.2.

[67] A. K. Hendrischk *et al.*, "A cryptochrome-like protein is involved in the regulation of photosynthesis genes in Rhodobacter sphaeroides," *Mol Microbiol*, vol. 74, no. 4, pp. 990–1003, Nov. 2009, doi: 10.1111/J.1365-2958.2009.06912.X.

[68] K. Jang, H. G. Kim, S. H. S. Hlaing, M. Kang, H. W. Choe, and Y. J. Kim, "A Short Review on Cryoprotectants for 3D Protein Structure Analysis," *Crystals 2022, Vol. 12, Page 138*, vol. 12, no. 2, p. 138, Jan. 2022, doi: 10.3390/CRYST12020138.

[69] J. M. Parkhurst *et al.*, "Background modelling of diffraction data in the presence of ice rings," *IUCrJ*, vol. 4, no. Pt 5, p. 626, Sep. 2017, doi: 10.1107/S2052252517010259.

APPENDIX

CCC Marketplace™

Order Number: 1248323
Order Date: 18 Jul 2022

Payment Information

Barış Çakılkaya
bcakilkaya14@ku.edu.tr
Payment method: Invoice

Billing Address:
Barış Çakılkaya
Zekeriyaköy mahallesi, Türkmen caddesi,
Sarıyer, Turkey
İstanbul, 34450
Turkey

+90 (530)9381220
bcakilkaya14@ku.edu.tr

Customer Location:
Barış Çakılkaya
Zekeriyaköy mahallesi, Türkmen caddesi,
Sarıyer, Turkey
İstanbul, 34450
Turkey

Order Details

1. Physical chemistry chemical physics

Billing Status: Open

Article: Dynamics and mechanisms of DNA repair by photolyase.

Order License ID	1248323-1	**Type of use**	Republish in a thesis/dissertation
Order detail status	Completed		
ISSN	1463-9084	**Publisher**	ROYAL SOCIETY OF CHEMISTRY
		Portion	Image/photo/illustration

0.00 USD
Republication Permission

LICENSED CONTENT

Publication Title	Physical chemistry chemical physics	**Publication Type**	e-Journal
		Start Page	11933
Article Title	Dynamics and mechanisms of DNA repair by photolyase.	**End Page**	11949
		Issue	18
Author/Editor	Royal Society of Chemistry (Great Britain)	**Volume**	17
		URL	http://firstsearch.oclc.org/journal=1463-9076;screen=info;ECOIP
Date	01/01/1999		
Language	English		
Country	United Kingdom of Great Britain and Northern Ireland		
Rightsholder	Royal Society of Chemistry		

REQUEST DETAILS

Portion Type	Image/photo/illustration	**Distribution**	Worldwide

JOHN WILEY AND SONS LICENSE
TERMS AND CONDITIONS

Jul 17, 2022

This Agreement between Barış Çakılkaya ("You") and John Wiley and Sons ("John Wiley and Sons") consists of your license details and the terms and conditions provided by John Wiley and Sons and Copyright Clearance Center.

License Number	5351640177439
License date	Jul 17, 2022
Licensed Content Publisher	John Wiley and Sons
Licensed Content Publication	Photochemistry and Photobiology
Licensed Content Title	Repair of (6-4) Lesions in DNA by (6-4) Photolyase: 20 Years of Quest for the Photoreaction Mechanism
Licensed Content Author	Klaus Brettel, Pascal Plaza, Junpei Yamamoto
Licensed Content Date	Jan 31, 2017
Licensed Content Volume	93
Licensed Content Issue	1
Licensed Content Pages	16
Type of use	Dissertation/Thesis
Requestor type	University/Academic

JOHN WILEY AND SONS LICENSE
TERMS AND CONDITIONS

Jul 10, 2022

This Agreement between Barış Çakılkaya ("You") and John Wiley and Sons ("John Wiley and Sons") consists of your license details and the terms and conditions provided by John Wiley and Sons and Copyright Clearance Center.

License Number	5345321154936
License date	Jul 10, 2022
Licensed Content Publisher	John Wiley and Sons
Licensed Content Publication	Angewandte Chemie International Edition
Licensed Content Title	Mechanisms of DNA Repair by Photolyase and Excision Nuclease (Nobel Lecture)
Licensed Content Author	Aziz Sancar
Licensed Content Date	Jun 23, 2016
Licensed Content Volume	55
Licensed Content Issue	30
Licensed Content Pages	26
Type of use	Dissertation/Thesis
Requestor type	University/Academic
Format	Print and electronic